
IMPROVING THE INTERPRETABILITY OF GNN PREDICTIONS THROUGH CONFORMAL-BASED GRAPH SPARSIFICATION

Pablo Sánchez-Martín

Max Planck Institute for Intelligent Systems &
Saarland University
Tübingen/Saarbrücken, Germany
psanchez@tue.mpg.de

Kinaan Aamir Khan

McGill University
Montreal, Canada
kinaan.khan@mail.mcgill.ca

Isabel Valera

Saarland University
Max Planck Institute for Software Systems
Saarbrücken, Germany
ivalera@cs.uni-saarland.de

ABSTRACT

Graph Neural Networks (GNNs) have achieved state-of-the-art performance in solving graph classification tasks. However, most GNN architectures aggregate information from all nodes and edges in a graph, regardless of their relevance to the task at hand, thus hindering the interpretability of their predictions. In contrast to prior work, in this paper we propose a GNN *training* approach that jointly i) finds the most predictive subgraph by removing edges and/or nodes—*without making assumptions about the subgraph structure*—while ii) optimizing the performance of the graph classification task. To that end, we rely on reinforcement learning to solve the resulting bi-level optimization with a reward function based on conformal predictions to account for the current in-training uncertainty of the classifier. Our empirical results on nine different graph classification datasets show that our method competes in performance with baselines while relying on significantly sparser subgraphs, leading to more interpretable GNN-based predictions.

Keywords Graph Neural Networks · Interpretability · Conformal Prediction · Reinforcement Learning

1 Introduction

Graph Neural Networks (GNNs) have become a cornerstone in modern machine learning, excelling in diverse domains such as social network analysis Cao et al. [2019b,a], recommender systems Fan et al. [2019], Bai et al. [2020] and bioinformatics Guo et al. [2021], Ramirez et al. [2020], Xiong et al. [2020]. However, the complexity of GNNs contributes to one of their principal shortcoming: a lack of human-interpretable predictions. This opacity hinders their potential for practical, real-world impact, as practitioners often require interpretable models to inform decision-making, ensure trustworthiness, and comply with regulations Doshi-Velez and Kim [2017]. Current interpretability methods for GNN predictors aim to identify the most predictive subgraph from an original graph Sun et al. [2021]. In essence, interpretability in this context is closely tied to graph sparsity, implying the use of a minimal set of nodes and edges from the graph for prediction, rather than the entire graph \mathcal{G} .

This viewpoint of interpretability is exemplified in Figure 1 with the synthetic BA2Shapes dataset Ying et al. [2019]. In this dataset, a binary classification task can be solved using only specific motifs of the graphs (the house or the cycle motifs, i.e., yellow nodes), while the original graphs contain additional irrelevant information for the task at hand, i.e., purple nodes. A sparser graph reduces the volume of information used for making predictions, rendering it easier for humans to understand the GNN predictions. It is crucial to note that interpretability is achieved through sparsity only when the subgraph completely excludes information from the omitted nodes and edges since only then the subgraph,

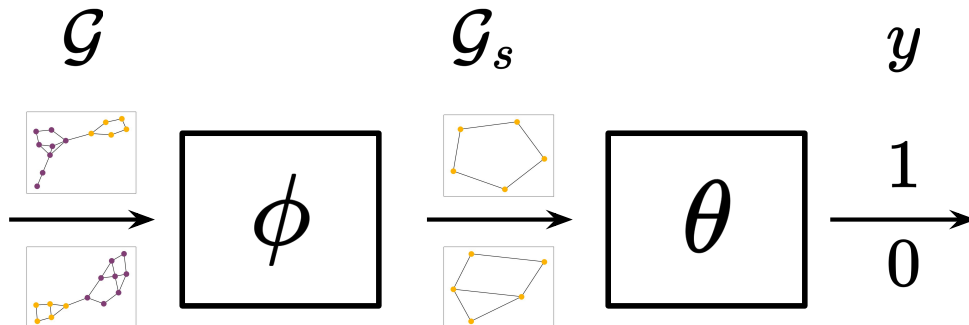


Figure 1: **CORES pipeline.** Illustration of the pipeline of CORES using the synthetic BA2Shapes designed for binary graph classification. On the left, we present two examples of original graphs, denoted as \mathcal{G} , corresponding to the positive class (top, cycle motif) and negative class (bottom, house motif). The policy ϕ of CORES takes \mathcal{G} and sparsifies it, resulting in the predictive subgraph \mathcal{G}_s , which retains only the relevant information for the task, i.e., the motifs. Finally, the graph classifier θ takes \mathcal{G}_s as input and produces the prediction $y \in \{0, 1\}$.

and thus, the explanation is *faithful* to the model prediction. This situation does not arise, for example, if message passing Kipf and Welling [2016] is applied to obtain the node embeddings before finding the subgraph.

While most of explainability methods for GNNs are post-hoc, some existing approaches attempt to identify the predictive subgraph during training Cangea et al. [2018], Sun et al. [2021]. These methods, however, exhibit two primary limitations: i) they often still rely on the entire graph for predictions Cangea et al. [2018], resulting in a lack of *faithfulness* to the model prediction (as described above), and/or ii) they impose strong assumptions concerning the structure of the predictive subgraph, such as a pre-defined size. In practical scenarios, relaxing assumptions on the subgraph structure is desirable. For instance, in community detection within social networks Contisciani et al. [2020], Shchur and Günnemann [2018], it is crucial to only remove edges connecting users across distinct communities but the number of inter-community connections varies significantly and is unknown a priori. Another relevant example is the prediction of mutagenic effects in compounds, where Debnath et al. [1991b] observed that diverse “motifs” of chemical elements are predictive. We refer the reader to Section 5 for a concrete example on the MUTAG dataset.

In this work, we introduce CORES, a novel algorithm for training GNNs that addresses the two fundamental challenges simultaneously: i) finding the informative subgraph \mathcal{G}_s by removing edges and/or nodes, *without imposing assumptions on the subgraph’s structure*, and ii) optimizing the performance of the graph classification task solely using the selected subgraph \mathcal{G}_s , thereby enhancing the interpretability of the classifier. To this end, we use a bi-level optimization approach. The optimization for performance adheres to the conventional supervised problem paradigm. We then apply reinforcement learning to identify the predictive subgraph, using a policy that allows edge and/or node removal modes. Our carefully designed reward function allows us to introduce inductive biases toward either sparse or high-performing solutions and uses conformal predictions Angelopoulos and Bates [2021] to account for classifier uncertainty at each training epoch.

In summary, our work presents the following key contributions: (i) A novel framework, CORES, which enables graph-level classification using only predictive subgraphs as input, leading to more interpretable solutions. (ii) The flexibility to choose between achieving sparsity through node or edge removal, which removes assumptions on the structure of the predictive subgraph and broadens the range of application scenarios. (iii) The design of a versatile reward function that takes into account the uncertainty of the classifier and allows to introduce inductive biases towards sparser or more high-performing solutions. (iv) A comprehensive comparison across nine graph classification datasets, showing that CORES makes predictions using significantly sparser graphs while keeping competitive performance.

2 Preliminaries

This section outlines necessary background information on the key building blocks of CORES: reinforcement learning, message-passing graph neural networks, and conformal predictions. We begin by introducing the notation used throughout this work.

Notation. A graph is denoted as $\mathcal{G} = (\mathcal{V}, \mathcal{E})$ where $\mathcal{V} \in \{1, \dots, n\} = [n]$ is the set of n nodes and $\mathcal{E} \subseteq \mathcal{V} \times \mathcal{V}$ is the set of edges. The size of a set is represented as $|\mathcal{V}|$. A subgraph of \mathcal{G} is denoted as $\mathcal{G}_s = (\mathcal{V}_s, \mathcal{E}_s) \subseteq \mathcal{G}$ comprising

subsets of nodes $\mathcal{V}_s \subseteq \mathcal{V}$ and edges $\mathcal{E}_s \subset \mathcal{E}$. A labeled dataset is represented as $\mathcal{D} = \{\mathcal{G}_i, \mathbf{y}_i\}_i$ where \mathbf{y}_i denotes the target of \mathcal{G}_i . Here, without loss of generality, we focus on K classes graph classification, hence $\mathbf{y}_i \in \{1, \dots, K\} = [K]$.

2.1 Reinforcement learning

Reinforcement Learning (RL) is a learning paradigm in which an agent learns to optimize decisions by interacting with an environment Sutton and Barto [2005]. The objective is to find a policy π that maximizes the expected cumulative reward. An RL problem is typically modeled as a Markov Decision Process (MDP), defined by a tuple $(\mathcal{S}, \mathcal{A}, \mathcal{P}, R, \gamma)$, where \mathcal{S} and \mathcal{A} denote the state and action spaces, \mathcal{P} the transition probability, R the reward function, and γ the discount factor.

Policy Gradient Methods. Policy gradient methods directly optimize the policy using gradient ascent on the expected cumulative reward Sutton et al. [1999]. Proximal Policy Optimization (PPO) Schulman et al. [2017b] is a policy gradient method that introduces an objective function fostering exploration while mitigating drastic policy updates. PPO aims to solve the optimization problem:

$$L^{CLIP}(\phi) = \mathbb{E}_t \left[\min \left(r_t(\phi) \hat{A}_t, \text{clip}(r_t(\phi), 1 - \epsilon, 1 + \epsilon) \hat{A}_t \right) \right] \quad (1)$$

where $r_t(\phi) = \frac{\pi_\phi(a_t|s_t)}{\pi_{\phi_{old}}(a_t|s_t)}$ is the probability ratio, \hat{A}_t an estimator of the advantage function at time t , and ϵ a hyperparameter controlling the deviation from the old policy.

2.2 Graph neural networks

Message passing Graph Neural Networks (GNNs) are designed for graph-structured data processing. Each node $v \in \mathcal{V}$ has a feature vector \mathbf{h} , and the GNN transforms these features using neighborhood information. Formally, a GNN performs L update rounds, updating each node's feature vector $\mathbf{h}_i^{(l)}$ at step $l \geq 1$:

$$\mathbf{h}_i^{(l)} = f_{\theta_u} \left(\bigoplus_{j \in \mathcal{N}_i} m_{\theta_m}(\mathbf{h}_i^{(l-1)}, \mathbf{h}_j^{(l-1)}) \right). \quad (2)$$

Here, f_{θ_u} and m_{θ_m} are differentiable, parameterized functions, \mathcal{N}_i represents node i 's neighbors, and \bigoplus denotes permutation invariant operations, i.e., sum, mean, or max. After L steps, we obtain the final node representations $\mathbf{h}_i^{(L)} \forall i \in \mathcal{V}$. These representations are used for tasks like graph-level prediction, employing a permutation-invariant readout function $\hat{\mathbf{y}} = g \left(\left\{ \mathbf{h}_i^{(L)} : i \in \mathcal{V} \right\} \right)$ that ensures the output is node order independent.

2.3 Conformal Prediction

Conformal prediction Angelopoulos and Bates [2021] is a framework that rigorously quantifies uncertainty in machine learning predictions. Given a labeled dataset $\{x_i, y_i\}_{i=1}^N$, a heuristic measure of uncertainty of our predictor (e.g., softmax values from a classifier f_θ), and a scoring function $s(x, y) \in \mathbb{R}$ that reflects prediction uncertainty, conformal prediction generates a prediction set for a new input x_{test} as follows:

$$\mathcal{C}(x_{\text{test}}) = \{y : s(x_{\text{test}}, y) \leq \hat{q}\} \subseteq [K]. \quad (3)$$

Here, \hat{q} represents the $\frac{\lceil (n+1)(1-\alpha) \rceil}{n}$ quantile of the calibration scores $\{s_i\}_n$, where α is a predefined error rate. In the context of classification tasks, one commonly used conformal procedure is Adaptive Prediction Sets (APS) Angelopoulos et al. [2020], Romano et al. [2020], which defines the scoring function as:

$$s(x, y) = \sum_{j=1}^k f_\theta(x) \pi_j(x), \text{ where } y = \pi_k(x) \quad (4)$$

Here, $\pi(x)$ represents the permutation of $[K]$ that arranges the softmax values $f_\theta(x)$ from most likely to least likely.

3 Related work

GNNs extend deep learning models to incorporate graph-structured data Bronstein et al. [2016]. Numerous architecture proposals have emerged, tailored for node, link, and graph prediction tasks Scarselli et al. [2009], Gilmer et al. [2017], Wu et al. [2019, 2020], Xu et al. [2018], Corso et al. [2020], Chen et al. [2020]. However, these approaches rely on the complete graph data and often disregard interpretability, which is the focus of our work. More recently, some works aim for sparsification Zheng et al. [2020], Hasanzadeh et al. [2020], Rong et al. [2019], Oono and Suzuki [2019], Loukas [2019], Li et al. [2020], Luo et al. [2021], Wickman et al. [2021], Wang et al. [2021]. However, these methods typically make strong assumptions on the predictive subgraph. Moreover, they often focus on tasks other than graph prediction.

Here, we explore relevant sparsification techniques that specifically target supervised problems, which are the main focus of our paper. We categorize these works into two categories: those employing soft information removal, where the predictive subgraph retains information from the complete graph, and thus may not be faithful to the model predictions; and those adopting hard information removal, which closely aligns with our approach.

Soft removal of information. Several architectures Javaloy et al. [2022], Velickovic et al. [2017], Brody et al. [2021] assign varying importance to network edges, simulating soft edge removal whilst maintaining information flow across nodes. DiffPool Ying et al. [2018] hierarchically removes parts of the original graph, distilling the graph’s representation into a single vector used for prediction. SAGPooling Lee et al. [2019], Knyazev et al. [2019], uses a GNN to update node features and subsequently selects the top k most relevant nodes based on their features. It is worth noting that even though part of the network is dropped, the remaining subgraph contains information from the entire network. In contrast, in our framework, the graph predictor does not have access to the dropped information.

Hard removal of information. GPool Gao and Ji [2019], Cangea et al. [2018], Knyazev et al. [2019] selects the top k nodes based solely on their information. However, the number of nodes is fixed and cannot dynamically change for different graphs. SUGAR Sun et al. [2021] takes a different approach by identifying discriminative subgraphs. It introduces a reinforcement pooling module trained with Q-learning Mnih et al. [2015] to adaptively select a pooling ratio when recombining subgraphs for classification. SUGAR also imposes a predefined size for the subgraphs. In contrast, CORES does not make any assumptions about the structure of the subgraph, uses policy gradient methods to capture uncertainty in the sparsity process, and allows for different modes of removal.

Finally, there is extensive literature that aims to understand which subgraph of the input graph is most relevant for making predictions in GNNs Ying et al. [2019], Luo et al. [2020], Yuan et al. [2020], Numeroso and Bacciu [2021], Yuan et al. [2021], Yu and Gao [2022], Schlichtkrull et al. [2021]. However, it is important to note that these methods primarily focus on explaining a GNN predictor trained using the original graphs. In contrast, our objective is to train a GNN that inherently utilizes a minimal portion of the original graph. While these methods may complement our approach by providing further insights of the predictions, they operate in a post-hoc manner.

4 CORES: Conformal-based reinforcement learning for graph sparsification

In this section, we present CORES, a novel training procedure for GNNs leveraging reinforcement learning with conformal-based rewards to achieve graph sparsification. Given a labeled dataset \mathcal{D} , the main goal of CORES is to identify a compact predictive subgraph $\mathcal{G}_s \subseteq \mathcal{G}$ that maintains high performance for a graph classification task. Next, we provide a detailed description of the different parts comprising CORES.

4.1 Optimizing for sparsity and performance

Firstly, we aim to learn a function $\pi_\phi : \mathcal{G} \mapsto \mathcal{G}_s$ with parameters ϕ responsible for identifying the predictive subgraph. This function corresponds to the policy of the reinforcement learning component of CORES. Secondly, we want to train a graph classifier $f_\theta : \mathcal{G}_s \rightarrow \hat{y}$ with parameters θ that takes the identified predictive subgraph as input and generates predictions. The pipeline of our approach is illustrated with the synthetic BA2Shapes dataset in Figure 1. To tackle this challenge we introduce a bi-level iterative optimization approach:

$$\phi^* = \arg \min_{\phi} \mathcal{L}_{\text{spa}}(\theta^*(\phi), \phi, \mathcal{D}^{val}) \quad (5)$$

$$\text{s.t. } \theta^*(\phi) = \arg \min_{\theta} \mathcal{L}_{\text{perf}}(\theta, \phi, \mathcal{D}^{tr}) \quad (6)$$

Algorithm 1 Training of CORES.

```
1: Input: Training  $\mathcal{D}^{tr}$  and validation  $\mathcal{D}^{val}$  sets; Initial graph classifier parameters  $\theta$  and policy parameters  $\phi$ ; Empty
   buffer  $\mathcal{B}$ ; Learning rates  $\alpha$  and  $\beta$ ; Number of PPO updates  $K$ 
2: while not convergence do
3:   for  $\{\mathbf{y}, \mathcal{G}\} \in \mathcal{D}^{tr}$  do                                     ▷ Get a (batch of) sample(s) from the training set
4:      $\pi_\phi : \mathcal{G} \mapsto \mathcal{G}_s$                                        ▷ Get the subgraph using the policy
5:      $\hat{\mathbf{y}}_s = f_\theta(\mathcal{G}_s)$                                            ▷ Get the prediction
6:      $\theta \leftarrow \theta - \alpha \nabla_\theta \mathcal{L}_{\text{perf}}(\theta, \phi)$        ▷ Update the parameters of the graph classifier
7:   end for
8:   for  $\{\mathbf{y}, \mathcal{G}\} \in \mathcal{D}^{val}$  do                                       ▷ Get a (batch of) sample(s) from the validation set
9:      $\pi_\phi : \mathcal{G} \mapsto \mathcal{G}_s$                                        ▷ Use the  $\pi$  to sample a sparse graph
10:     $\hat{\mathbf{y}}_s = f(\mathcal{G}_s)$                                            ▷ Get the prediction of the sparse graph
11:    Add tuple  $\{\mathbf{y}, \mathcal{G}, \hat{\mathbf{y}}, \mathcal{G}_s\}$  to the buffer  $\mathcal{B}$ 
12:  end for
13:  Compute the quantile  $\hat{q}$  using the calibration scores obtained with  $\mathcal{D}^{tr}$ 
14:  Compute rewards and prepare mini-batches from buffer  $\mathcal{B}$  for PPO updates
15:  for  $i = \{1, 2, \dots, K\}$  do                                           ▷ Update PPO  $K$  times
16:     $\{\mathbf{y}, \mathcal{G}, \hat{\mathbf{y}}, \mathcal{G}_s, r\} \sim \mathcal{B}$                                ▷ Sample a batch of tuples from the buffer
17:    Compute advantage estimates  $\hat{A}$ 
18:     $\phi \leftarrow \phi - \beta \nabla_\phi \mathcal{L}_{\text{spa}}(\theta, \phi)$            ▷ Update policy by maximizing Equation (1)
19:  end for
20:  Check for convergence, update convergence flag
21: end while
22: Output: Optimal policy parameters  $\phi$  and graph classifier parameters  $\theta$ 
```

The nested structure of the problem implies that achieving an optimal predictive subgraph requires a high-performing graph classifier. We employ gradient descent for both optimizations, with a larger learning rate for the inner optimization Zheng et al. [2021]. Also, notice that we use the training \mathcal{D}^{tr} and validation \mathcal{D}^{val} sets to solve the inner and outer procedures respectively, which avoids overfitting. Algorithm 1 summarizes the training procedure.

Performance optimization. This objective corresponds to Equation (6) which represents a standard graph-supervised problem. Here, the objective is to minimize a loss function $\mathcal{L}_{\text{perf}}$, e.g., the cross-entropy loss. Thus the goal is to learn a function $f_\theta : \mathcal{G}_s \rightarrow \hat{\mathbf{y}}$ with parameters θ that minimizes the prediction loss.

Sparsity optimization . This optimization task corresponds Equation (5). It presents a considerable challenge due to the combinatorial nature of the node and edge removal process. Specifically, we must determine both which edges $((u, v) \in \mathcal{E})$ and/or nodes $(v \in \mathcal{V})$ and how many of them, should be removed. Drawing inspiration from SparRL Wickman et al. [2021], we formulate the sparsification task as a Markov Decision Process (MDP) and address it through the framework of graph reinforcement learning Nie et al. [2022]: we parameterize the policy π_ϕ using a GNN. In contrast to prior approaches that rely on value-based methods like Deep Q-Learning Mnih et al. [2015], we opt for the policy gradient method Proximal Policy Optimization (PPO) Schulman et al. [2017a] to capture the inherent uncertainty in the sparsification process. We denote the objective of sparsity optimization as \mathcal{L}_{spa} , which corresponds to solving the PPO objective in Equation (1). The outcome of this task is a policy π_ϕ that finds the predictive subgraph \mathcal{G}_s , subsequently employed as input for the graph classification task. Next, we provide more details on the sparsity optimization.

4.2 Unpacking the sparsity optimization

In this subsection, we provide a detailed description of the components of the PPO method we designed to identify the predictive subgraph. In RL problems, agents usually make sequential decisions over multiple time steps, and the rewards they receive at each step may depend on the whole trajectory taken so far. This challenge, known as the “delayed reward” problem, is a central challenge in RL Sutton [1992]. Our objective shifts towards identifying the predictive subgraph in a single step, rather than considering a trajectory as in traditional RL. This approach aims to find a strategy that maximizes the reward across the dataset graphs. This simplified scenario resembles the Multi-Armed Bandit Problem Kuleshov and Precup [2014]. As our experiments in Section 5 empirically show, this simplified scenario effectively achieves high-performance relying on significantly sparser graphs. Below, we focus on describing two key

components: the policy responsible for the removal process and the design of the reward function that guides the policy in finding the optimal predictive subgraph.

4.2.1 Policy formulation for graph sparsification via node or edge removal

We propose a policy $\pi(\mathbf{a}|\mathcal{G}; \phi)$ we model using a GNN with parameters ϕ . Given an input graph \mathcal{G} , the policy produces an action \mathbf{a} , where each element determines whether to keep ($a_i = 0$) or remove ($a_i = 1$) a specific node or edge in \mathcal{V} or \mathcal{E} , respectively. This action results in a subgraph $\mathcal{G}_s \subseteq \mathcal{G}$. Recognizing the inherent uncertainty in real-world scenarios where the importance of a node/edge may not be clear, we design the policy as a probability distribution. We establish two operational modes depending on the removal objective:

- **Node Removal Policy:** $\pi_n(\mathbf{a}|\mathcal{G}; \phi)$, where $\mathbf{a} \in \{0, 1\}^{|\mathcal{V}|}$. In this scenario, the resulting subgraph \mathcal{G}_s , used as input for the downstream task, satisfies $\mathcal{V}_s = \{v \in \mathcal{V} | a_v = 0\}$ and $\mathcal{E}_s = \{(u, v) \in \mathcal{E} | a_u = 0 \wedge a_v = 0\}$.
- **Edge Removal Policy:** $\pi_e(\mathbf{a}|\mathcal{G}; \phi)$, where $\mathbf{a} \in \{0, 1\}^{|\mathcal{E}|}$. Here, the subgraph \mathcal{G}_s , used as input for the downstream task, has $\mathcal{V}_s = \mathcal{V}$ and $\mathcal{E}_s = \{(u, v) \in \mathcal{E} | a_{uv} = 0\}$.

Note that node removal implies the removal of all edges connected to the node. In contrast, the edge removal policy retains all nodes, making it suitable for node classification, which is a direction for future work. In either case, determining \mathcal{G}_s poses an NP-hard problem for both removal modes. The number of potential subgraphs increases exponentially with the number of nodes/edges in the original graph. Specifically, the number of possible actions for π_n is $\sum_{i=1}^{|\mathcal{V}|-1} \binom{|\mathcal{V}|}{i}$, while for π_e , it is $\sum_{i=1}^{|\mathcal{E}|} \binom{|\mathcal{E}|}{i}$. RL can be helpful to solve combinatorial problems, particularly when the reward function effectively guides the optimization process Mazyavkina et al. [2020].

4.2.2 Reward formulation

The reward function R plays a pivotal role in shaping the policy’s behavior. It should provide positive rewards for predictive and sparse subgraphs while penalizing those that negatively impact the performance of the graph classifier. It is also important to consider that the classifier makes errors, i.e., it does not achieve perfect performance. Consequently, there are instances where a subgraph may be genuinely predictive, but the classifier produces an incorrect prediction. Our reward design accounts for this inherent uncertainty through the use of conformal predictions, as described in a subsequent section. It consists of two primary components: one aimed at enhancing performance and the other dedicated to promoting sparsity.

Performance Reward (R_p). Our approach to rewarding performance is straightforward. We simply use the softmax score assigned by the graph classifier to the correct class y , i.e., $R_p = f_\theta(\mathcal{G}_s)_y \in [0, 1]$.

Sparsity Reward (R_s). To incentivize a minimal predictive subgraph, we introduce a component that penalizes the *nodes ratio* $PR_n = \frac{|\mathcal{V}_s|}{|\mathcal{V}|}$ or the *edges ratio* $PR_e = \frac{|\mathcal{E}_s|}{|\mathcal{E}|}$ kept from the original graph, depending on the policy mode. To control the desired sparsity level, we introduce a parameter $d \in [0, 1]$ representing the *maximum desired nodes/edges ratio*. Then, we define the sparsity reward as $R_s(\mathcal{G}_s) = 1 - PR^{\tilde{d}}$, where \tilde{d} is a transformation of d such that $R_s = 0.95$ when $PR = d$. The variation of R_s with respect to PR for different d values is depicted in the inline figure. Each vertical line represents a unique d value, extending upwards until $R_s = 0.95$ for all instances.

To seek sparsity, a smaller d value (e.g., blue or yellow curves) is preferred. This leads to a slower increase in R_s with node/edge removal, rewarding substantial removal. Conversely, when d approaches 1 (e.g., pink curve), R_s close to 1 are awarded even for keeping most nodes/edges.

Note that both reward components fall within the range $[0, 1]$, facilitating comparison. Now, we proceed to define the reward function used in CORES:

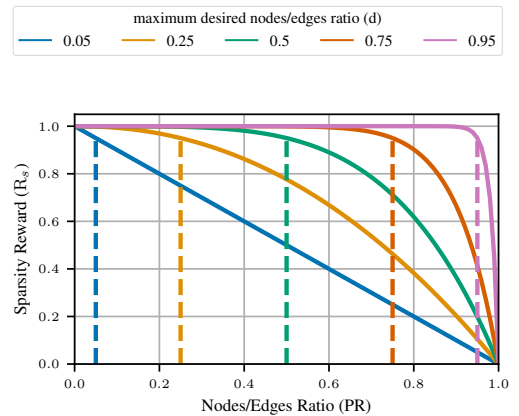


Figure 2: Evolution of the sparsity reward R_s over the node/edge ratio for different values of the *maximum desired nodes/edges ratio* d .

Table 1: Statistics of the datasets.

Dataset	# Graphs	# Features	# Edge Features	# Classes	Undirected	# Nodes	# Edges
BZR	405	10	0	2	Yes	35.75 ± 7.26	76.72 ± 15.39
COX2	467	10	0	2	Yes	41.22 ± 4.03	86.89 ± 8.53
DD	1178	20	0	2	Yes	284.32 ± 272.00	1431.32 ± 1387.81
ENZYMES	600	21	0	6	Yes	32.63 ± 15.28	124.27 ± 51.00
MUTAG	135	7	4	2	Yes	18.85 ± 4.49	41.67 ± 11.13
NCI1	4110	7	0	2	Yes	29.87 ± 13.56	64.60 ± 29.87
NCI109	4127	8	0	2	Yes	29.68 ± 13.57	64.26 ± 29.92
PROTEINS	1113	4	0	2	Yes	39.06 ± 45.76	145.63 ± 169.20
PTC	349	8	4	2	Yes	14.11 ± 8.44	28.97 ± 18.88

$$R = \begin{cases} \lambda R_p + (1 - \lambda) R_s(\mathcal{G}_s) & \text{if } y \in \mathcal{C}(\mathcal{G}_s) \wedge |\mathcal{C}(\mathcal{G}_s)| = 1, \\ \frac{R_p}{|\mathcal{C}(\mathcal{G}_s)|} & \text{if } y \in \mathcal{C}(\mathcal{G}_s) \wedge |\mathcal{C}(\mathcal{G}_s)| > 1, \\ -R_s(\mathcal{G}_s) & \text{if } y \notin \mathcal{C}(\mathcal{G}_s). \end{cases} \quad (7)$$

There are two key aspects to highlight. Firstly, we compute the quantile \hat{q} used to obtain the prediction set \mathcal{C} using the scoring function introduced in Equation (4). Secondly, it involves three different cases based on whether the true label y is within the prediction set and the size of the prediction set.

The top scenario corresponds to cases in which the predictive subgraph leads to a highly certain and correct prediction. Here, a parameter $\lambda \in [0, 1]$ allows practitioners to emphasize either performance ($\lambda = 1$) or sparsity ($\lambda = 0$). In this scenario, the reward is in the range $R \in [0, 1]$. The middle scenario addresses instances in which the subgraph leads to the classifier being uncertain about the prediction, i.e., $|\mathcal{C}(\mathcal{G}_s)| > 1$. In such cases, we aim to provide a positive but smaller reward within the range $(0, 0.5)$. This reward encourages to increase the probability of the true label and to reduce the size of the prediction set, that is moving to the top scenario. Intuitively, this scenario arises with challenging examples. The bottom scenario refers to cases in which the predictive subgraph results in an incorrect prediction, falling outside the prediction set \mathcal{C} . As this behavior is undesirable, the rewards R fall within the range $[-1, 0]$, encouraging to reduce sparsity. In this scenario, the reward reaches 0 only when we recover the original graph.

The use of conformal prediction in the reward function is essential to guide the policy toward discovering a good predictive subgraph. If the task is challenging and the classifier exhibits uncertainty, the focus should initially be on performance. Only when the classifier is confident about the prediction should we encourage sparsity. In the following section, we present empirical evidence supporting the reward function’s design, and more generally our approach CORES, for achieving both performance and compact predictive subgraphs.

5 Experiments

In this section, we present a comprehensive set of experiments to assess the performance of CORES. First, we conduct an ablation study to show the impact of different values of λ and maximum desired ratio (d) on performance, as well as the effect of the choice of base GNN architecture. Then, we compare CORES with relevant baselines.

Proposed approaches. We evaluate the two information removal modes of the proposed framework, described in Section 4.2.1. We denote the model with the policy that removes nodes as CORES_N and the model with the policy that exclusively removes edges as CORES_E.

Datasets. In this study, we used seven Bioinformatics datasets, which include MUTAG Debnath et al. [1991a], DD Dobson and Doig [2003], ENZYMES Borgwardt et al. [2005], NCI1 Wale et al. [2006], NCI109 Wale et al. [2006], PTC Toivonen et al. [2003], and PROTEINS Borgwardt et al. [2005]. Additionally, we incorporated two chemical compound datasets, BZR Fey and Lenssen [2019a] and COX2 Fey and Lenssen [2019a]. Table 1 shows the statistics of the datasets.

Experimental setup. Aiming for computational efficiency, we conducted cross-validation on the hyperparameters of the vanilla GNN classifier, i.e., the GNN architecture (e.g., GIN) trained with stochastic gradient descent. We selected the optimal configuration of hyperparameters based on the validation set and used it to train the remaining models. We performed 5-fold cross-validation and reported standard deviation values on the test set at the last epoch.

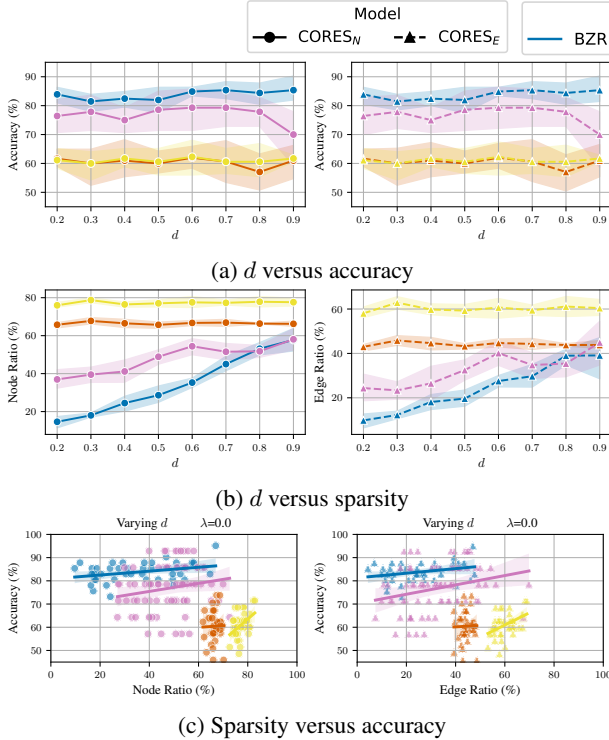


Figure 3: **Ablation study on the maximum desired ratio d .** We use the GIN architecture and run each experiment for 5 different folds.

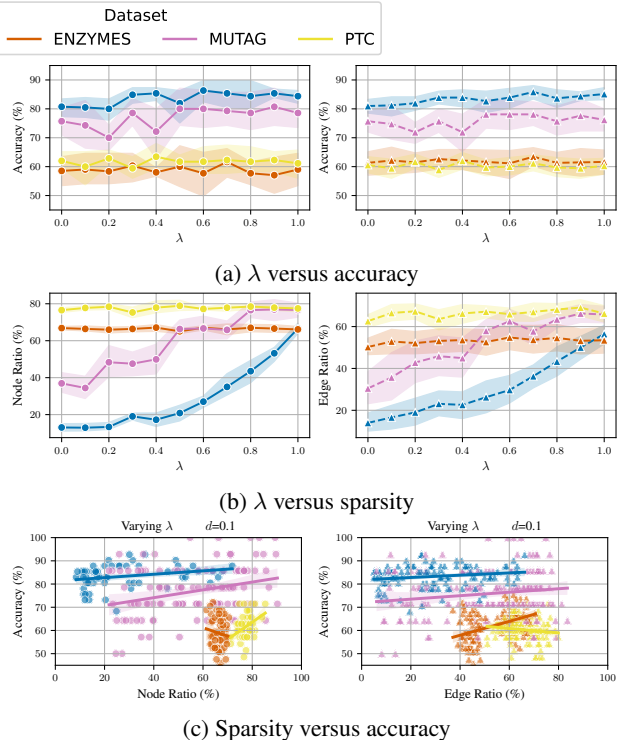


Figure 4: **Ablation study on λ .** We use the GIN architecture and run each experiment for 5 different folds.

All experiments were conducted on a single CPU with 8GB of RAM. Here, we present results obtained using the GIN architecture. Additional results using other well-known architectures, namely GAT and GCN, are provided in Appendix C. For a comprehensive overview of the best configuration hyperparameters obtained for each model, architecture and dataset, please refer to Appendix A. We implemented the baselines using the Torch Geometric package Fey and Lenssen [2019b] whenever it was available. Furthermore, we provide the implementation of CORES, along with the necessary scripts to replicate the experiments, at <https://github.com/psanch21/CORES>.

5.1 Ablation study

In this section, we provide an ablation study on the proposed framework analyzing the effects of key hyperparameters and different choices for the base GNN architecture.

Analysis of the impact of λ and d . The reward function, presented in Equation (7), leverages two hyperparameters: the maximum desired nodes/edges ratio (d) and the balancing parameter (λ) to prioritize performance or sparsity. For the nine datasets under study, we present the effect of varying d and λ in Figure 3 and Figure 4, respectively, for both CORES_N (solid lines) and CORES_E (dashed lines). For this ablation study, we use GIN as the base GNN architecture. The results are color-coded for each dataset. The figures in the top row contain the performance analysis, while the middle row shows the sparsity, specifically the node ratio ($\frac{|V_s|}{|V|}$) for CORES_N and the edge ratio ($\frac{|E_s|}{|E|}$) for CORES_E. The bottom row shows performance versus sparsity in the vertical and horizontal axes respectively.

In Figure 3, we fix $\lambda = 0.0$ (only rewarding sparsity) while varying d within the range $[0.2, 0.9]$. Regarding performance (top row), we observe that generally, the value of d does not have an impact. The middle row, which focuses on sparsity, reveals interesting variations among datasets. For instance, for the MUTAG dataset, CORES finds a predictive subgraph that utilizes as little as 20% of the original nodes/edges with $d = 0.2$. In contrast, for the PTC dataset, we keep approximately 80% of the original nodes in CORES_N and 60% of the original edges in CORES_E, even with low d values. The bottom figures highlight that for certain datasets, e.g., BZR, CORES can maintain comparable accuracy regardless of sparsity levels. Conversely, for other datasets, decreasing sparsity tends to enhance performance, such as the case with the PTC dataset and CORES_N. These findings suggest that some datasets exhibit rapid performance

Table 2: **Ablation study on GNN architecture.** We compare the performance (accuracy) and sparsity (node/edge ratio) of CORES with the Vanilla approach for the GCN (left) and GAT(right) architectures. We show the mean over 5 independent runs and the standard deviation as the subindex. All metrics are shown in percentages.

Dataset	Metric	GCN			GAT		
		Vanilla	CORES _N	CORES _E	Vanilla	CORES _N	CORES _E
BZR	Accuracy	86.83 _{4.08}	82.44 _{4.69}	80.98 _{5.29}	80.98 _{4.36}	83.90 _{4.43}	81.46 _{4.08}
	Node Ratio	-	76.98 _{6.06}	100.00 _{0.00}	-	37.99 _{10.27}	100.00 _{0.00}
	Edge Ratio	-	61.17 _{11.31}	46.16 _{5.68}	-	29.92 _{8.83}	57.26 _{21.50}
COX2	Accuracy	79.15 _{4.85}	80.85 _{3.01}	81.70 _{4.90}	82.13 _{4.15}	81.70 _{4.41}	80.85 _{2.61}
	Node Ratio	-	72.49 _{4.24}	100.00 _{0.00}	-	77.91 _{2.29}	100.00 _{0.00}
	Edge Ratio	-	53.19 _{8.07}	31.27 _{23.60}	-	62.62 _{3.24}	66.18 _{0.38}
DD	Accuracy	78.47 _{3.47}	79.32 _{2.58}	75.76 _{4.05}	76.10 _{3.02}	75.42 _{4.19}	76.44 _{2.19}
	Node Ratio	-	56.44 _{2.50}	100.00 _{0.00}	-	75.16 _{1.39}	100.00 _{0.00}
	Edge Ratio	-	32.01 _{2.89}	51.39 _{1.90}	-	56.42 _{2.16}	58.62 _{2.51}
ENZYMES	Accuracy	66.00 _{5.35}	58.31 _{8.47}	57.02 _{11.62}	71.33 _{10.63}	69.84 _{4.43}	67.54 _{12.23}
	Node Ratio	-	77.17 _{7.28}	100.00 _{0.00}	-	80.26 _{1.03}	100.00 _{0.00}
	Edge Ratio	-	62.33 _{9.26}	74.20 _{35.99}	-	65.92 _{1.80}	61.60 _{9.06}
MUTAG	Accuracy	81.43 _{3.91}	81.43 _{10.83}	87.14 _{6.56}	81.43 _{6.39}	80.00 _{5.98}	81.43 _{6.02}
	Node Ratio	-	79.94 _{2.79}	100.00 _{0.00}	-	75.72 _{4.04}	100.00 _{0.00}
	Edge Ratio	-	63.52 _{4.23}	32.66 _{8.79}	-	58.74 _{6.05}	55.25 _{14.77}
NCI1	Accuracy	77.33 _{2.09}	66.45 _{7.71}	65.94 _{6.31}	79.42 _{1.34}	73.43 _{2.67}	75.38 _{1.22}
	Node Ratio	-	76.47 _{17.88}	100.00 _{0.00}	-	63.49 _{3.58}	100.00 _{0.00}
	Edge Ratio	-	64.02 _{18.84}	37.98 _{14.34}	-	53.33 _{2.81}	88.68 _{6.67}
NCI109	Accuracy	79.32 _{1.57}	76.08 _{2.71}	77.14 _{2.02}	76.90 _{1.34}	74.72 _{2.25}	72.78 _{2.29}
	Node Ratio	-	78.78 _{4.15}	100.00 _{0.00}	-	71.55 _{11.30}	100.00 _{0.00}
	Edge Ratio	-	67.08 _{4.42}	92.02 _{1.93}	-	62.37 _{12.96}	62.37 _{13.13}
PROTEINS	Accuracy	72.86 _{1.02}	73.21 _{2.45}	75.89 _{1.94}	75.36 _{3.00}	73.39 _{3.86}	73.57 _{1.62}
	Node Ratio	-	74.66 _{6.10}	100.00 _{0.00}	-	67.94 _{2.97}	100.00 _{0.00}
	Edge Ratio	-	56.12 _{9.77}	64.73 _{0.98}	-	46.56 _{4.27}	52.82 _{1.86}
PTC	Accuracy	57.78 _{7.71}	62.86 _{2.86}	63.43 _{3.13}	64.00 _{4.33}	62.96 _{4.17}	59.43 _{4.69}
	Node Ratio	-	64.10 _{4.19}	100.00 _{0.00}	-	45.61 _{6.00}	100.00 _{0.00}
	Edge Ratio	-	40.21 _{6.93}	44.47 _{5.29}	-	21.24 _{6.53}	76.36 _{14.75}

degradation when information is removed. Examining the different reward scenarios in our reward definition (refer to Equation (7)), it is intuitive to deduce that CORES will prioritize reducing sparsity if the prediction is not within the prediction set (bottom scenario) or enhancing performance when the classifier exhibits uncertainty (middle scenario).

In Figure 4, we fix $d = 0.1$ (favoring high levels of sparsity) and we vary λ within the range $[0.0, 1.0]$. We observe a similar behavior as in Figure 3. The top row consistently shows that varying λ has a minimal impact on accuracy, and only sometimes leads to increased accuracy as λ increases (e.g., BZR dataset). Importantly, for none of the datasets does performance degrade with higher λ values. This behavior aligns with our objective, as higher values of λ correspond to a greater emphasis on rewarding performance. The middle row reveals two distinct patterns: i) a high correlation between λ and the number of nodes/edges kept, particularly evident in datasets like MUTAG, and ii) minimal sensitivity, as observed with the PTC dataset. The bottom row reveals similar patterns: positive correlation between the node/edge ratio and accuracy. It is also worth noting that varying λ results in a wide range of sparsity levels for some datasets, such as 20-90% for MUTAG, and a narrower range for others, like 40-70% for PTC.

In summary, we observe that varying d or λ leads to one of two scenarios, depending on the dataset: i) A minimal change in performance and low sparsity, which suggests that information removal significantly degrades performance for these datasets. ii) A small positive correlation between the hyperparameters and performance and a high negative correlation between the hyperparameters and sparsity. Based on these insights, we recommend that practitioners use d to fine-tune sparsity levels and consider $\lambda = 1.0$ when prioritizing performance over sparsity. Appendix B contains the results for the rest of the datasets under study.

Table 3: **Model comparison results.** We show the mean over 5 independent runs and the standard deviation as the subindex. All metrics are shown in percentage. The last rows include the average ranking of the model across datasets. Best performing models on average are indicated in bold.

Dataset	Metric	Full Models			Sparse Models			
		Vanilla	SAGPool	DiffPool	SUGAR	GPool	CORES _N	CORES _E
BZR	Accuracy	82.44 _{5.00}	85.85 _{2.67}	70.24 _{5.95}	-	80.98 _{4.01}	84.88 _{4.01}	81.95 _{5.62}
	Node Ratio	-	-	-	-	96.46 _{0.19}	15.91 _{5.30}	100.00 _{0.00}
	Edge Ratio	-	-	-	-	96.40 _{0.45}	10.84 _{5.80}	76.03 _{3.72}
COX2	Accuracy	82.13 _{5.12}	80.43 _{3.16}	65.83 _{6.65}	-	80.43 _{3.50}	82.98 _{3.36}	85.11 _{3.01}
	Node Ratio	-	-	-	-	91.15 _{0.14}	86.44 _{3.48}	100.00 _{0.00}
	Edge Ratio	-	-	-	-	89.20 _{1.08}	77.63 _{6.60}	58.30 _{28.00}
DD	Accuracy	78.81 _{3.44}	74.07 _{4.09}	-	-	77.46 _{3.31}	75.42 _{5.22}	75.25 _{2.77}
	Node Ratio	-	-	-	-	40.23 _{0.03}	47.53 _{15.04}	100.00 _{0.00}
	Edge Ratio	-	-	-	-	15.41 _{0.26}	25.88 _{14.79}	51.55 _{2.42}
ENZYMES	Accuracy	61.67 _{8.50}	45.90 _{5.18}	31.00 _{6.66}	16.67 _{23.57}	62.62 _{5.36}	62.33 _{6.08}	64.92 _{3.40}
	Node Ratio	-	-	-	-	96.67 _{0.14}	80.67 _{1.16}	100.00 _{0.00}
	Edge Ratio	-	-	-	-	93.37 _{0.14}	66.90 _{1.66}	72.71 _{1.00}
MUTAG	Accuracy	85.71 _{8.75}	78.57 _{5.05}	69.00 _{12.21}	76.34 _{3.80}	81.43 _{3.91}	82.86 _{6.39}	82.14 _{5.98}
	Node Ratio	-	-	-	-	51.38 _{0.12}	52.38 _{7.67}	100.00 _{0.00}
	Edge Ratio	-	-	-	-	36.56 _{9.20}	36.31 _{11.32}	61.09 _{12.39}
NCI1	Accuracy	76.89 _{2.03}	69.29 _{2.12}	69.93 _{3.24}	49.95 _{35.58}	77.77 _{1.93}	73.34 _{6.30}	74.34 _{7.53}
	Node Ratio	-	-	-	-	96.89 _{0.08}	89.13 _{13.88}	100.00 _{0.00}
	Edge Ratio	-	-	-	-	94.47 _{0.28}	86.61 _{20.20}	84.06 _{27.86}
NCI109	Accuracy	78.64 _{2.69}	74.14 _{0.85}	67.49 _{2.60}	49.65 _{35.71}	75.45 _{3.30}	73.03 _{1.90}	75.74 _{2.04}
	Node Ratio	-	-	-	-	96.79 _{0.04}	66.31 _{5.69}	100.00 _{0.00}
	Edge Ratio	-	-	-	-	93.65 _{0.22}	61.26 _{7.22}	71.34 _{7.62}
PROTEINS	Accuracy	75.18 _{2.04}	70.54 _{3.63}	66.42 _{7.19}	59.57 _{43.01}	72.68 _{1.85}	73.75 _{4.02}	74.11 _{2.82}
	Node Ratio	-	-	-	-	41.92 _{0.30}	87.01 _{20.04}	100.00 _{0.00}
	Edge Ratio	-	-	-	-	19.42 _{0.64}	78.55 _{32.05}	83.31 _{37.32}
PTC	Accuracy	63.43 _{1.28}	61.14 _{8.23}	54.44 _{11.10}	56.14 _{8.95}	59.43 _{3.73}	64.00 _{3.26}	63.43 _{1.28}
	Node Ratio	-	-	-	-	43.52 _{0.67}	96.02 _{8.80}	100.00 _{0.00}
	Edge Ratio	-	-	-	-	24.80 _{3.48}	93.19 _{15.13}	88.61 _{15.64}
Avg. Rank	Accuracy	2.11	4.44	6.12	6.67	3.44	2.67	2.67
	Node Ratio	-	-	-	-	1.56	1.44	-
	Edge Ratio	-	-	-	-	2.22	1.67	2.11

Ablation on the base GNN architecture. Now, we analyze how switching the base architecture affects the performance of CORES. Table 2 summarizes the results for two base architectures: GCN and GAT. We observe that even when the base architecture changes, both CORES_N and CORES_E achieve competitive accuracy compared to the respective Vanilla approach that simply trains the GNN architecture using all the information from the original graph. We refer the reader to Appendix C for the complete results.

5.2 Performance comparison

In this section, we conduct a comprehensive evaluation of CORES by comparing it with baselines and competing methods across nine datasets.

We assess the performance on the test set using three key metrics: accuracy (the larger the better \uparrow), as well as the percentage of nodes (for CORES_N) or edges (for CORES_E) kept in the subgraph (the lower the better \downarrow). Decreasing these percentages increases graph sparsity, enhancing model interpretability.

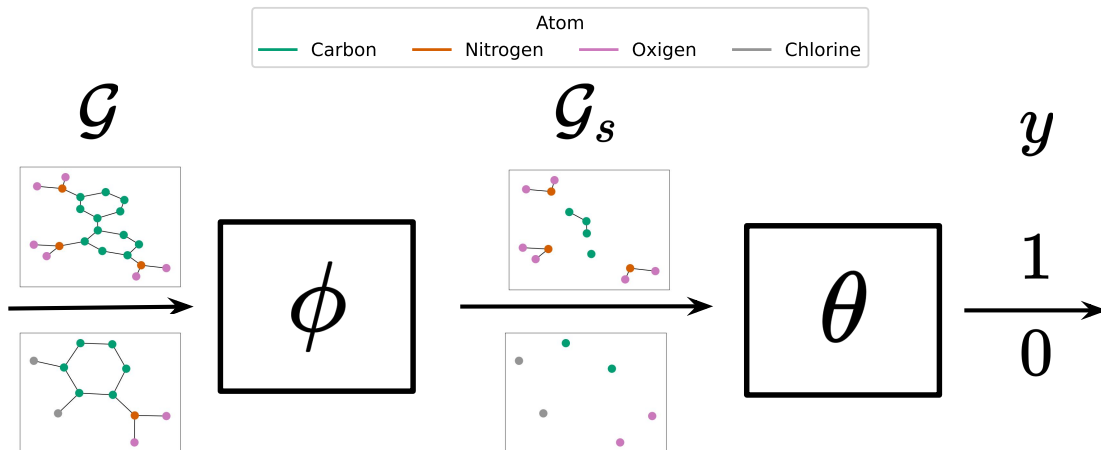


Figure 5: Illustration of the predictive subgraph obtained by CORES_N for a mutagenic (top) and non-mutagenic (bottom) graph of the MUTAG dataset.

Baselines. We divided the baselines into two categories: *Full* model (use complete graph information) and *Sparse* (use part of the graph information) model approaches. In the *Full* model category, we compare with the following approaches: Vanilla approach representing training the base GNN architecture without any sparsity consideration, DiffPool Ying et al. [2018], and SAGPooling Lee et al. [2019], Knyazev et al. [2019]—which uses node embeddings coming from a GNN to select the top k nodes, thus incorporating global information. For the *Sparse* models, we compare with: SUGAR Sun et al. [2021]¹ (for the datasets that their code can run) and GPool Gao and Ji [2019], Cangea et al. [2018], Knyazev et al. [2019]—where the node embeddings used to select the top k come from a multi-layer perceptron, hence the subgraph does not contain global information. Here, we present the results using GIN Xu et al. [2018] as the base GNN architecture. Refer to Appendix C for the results using GCN and GAT.

Quantitative results. Table 3 summarizes the results. In terms of accuracy, we observe that while Vanilla consistently achieves the highest accuracy on most datasets, CORES_E and CORES_N secure the second and third-best positions, outperforming all other *Full* models and all *Sparse* models, which highlights the competitive performance of the proposed approach. On the other hand, SUGAR consistently underperforms across all datasets, and its results exhibit high variance. Regarding interpretability (understood as sparsity), we perform a node and edge ratio analysis on the three best-performing *Sparse* models in terms of accuracy: CORES_N, CORES_E, and GPool. It is important to note that CORES_E consistently maintains a node ratio of 100%, due to its edge removal strategy that preserves all nodes. Among these models, CORES_N achieves the highest rankings in both node and edge ratios, indicating its effectiveness in removing a larger number of nodes from the original graph. Consequently, the graph classifier operates on a reduced, and thus more interpretable, subgraph. Finally, we find it interesting to analyze the results for the PTC dataset (bottom row). We observe that CORES, in both removal modes, achieves the worst sparsity results but at the same time the best performance among all models. In terms of sparsity, CORES_N keeps 96.02% of the nodes, while CORES_E keeps 88.61% of the edges. In terms of accuracy, all the models achieve less than 65%, which is notably low for a binary classification problem. This indicates that the classifier makes a substantial number of errors. This observation is important considering the design of the proposed reward function of CORES (see Equation (7)). For this dataset, the reward function places CORES in a scenario where it seeks to enhance performance, corresponding to the middle case, or penalize sparsity, corresponding to the bottom case of the reward function. In essence, CORES behaves in accordance with the reward function.

Qualitative results. Figure 5 presents two examples of the predictive subgraphs discovered by CORES_N for the MUTAG dataset, showcasing positive (top) and negative (bottom) instances. In this dataset, the positive class ($y = 1$) represents mutagenic molecules, while the negative class ($y = 0$) corresponds to non-mutagenic molecules. The left side of the figure shows the original graphs, while the center illustrates the predictive subgraphs identified by CORES_N. We observe that for the mutagenic graph (top), CORES_N keeps N_2 nitrogen dioxide compounds and some carbon

¹We use the official implementation of SUGAR to extract the results on the above datasets. We believe our evaluation of a held-out test set may explain the disparity between the results we report and those in Sun et al. [2021]. Instead, the available implementation of SUGAR evaluates on the same validation set used to select the best model.

atoms, while for the non-mutagenic graph (bottom), it captures chlorine carbon atoms as relevant for the classification task. These findings align with prior in the chemical domain Debnath et al. [1991b].

Time complexity. Training and inference are significantly faster in methods that employ a straightforward forward pass compared to RL-based methods like SUGAR and CORES. Notably, our findings indicate that CORES is at least as fast as SUGAR during training and can be up to 10 times faster during inference. For comprehensive quantitative results across all datasets, please refer to Appendix D.

6 Conclusions

Graph Neural Networks (GNNs) have demonstrated exceptional performance in graph-level tasks, but suffer from interpretability issues due to their complexity. Existing interpretability research in GNNs mainly focuses on post-hoc explanations. Approaches that aim to introduce *sparsity* during training often provide predictive subgraphs that are not *faithful* with the classifier predictions. Also, these methods often rely on complete graph information and/or make strong assumptions about the sparser graphs. In this work, we introduced CORES, a novel GNN training approach that simultaneously identifies predictive subgraphs by removing edges and/or nodes, without imposing assumptions about subgraph structures; and optimizes the performance of the graph classification task. The optimization for performance refers to the conventional supervised problem paradigm. We then leverage reinforcement learning to identify predictive subgraphs, using a policy that allows both edge and node removal modes. One key aspect of CORES is the design of the reward function. This function allows the practitioner to introduce inductive biases towards either sparse or high-performing predictive subgraphs and it incorporates conformal predictions Angelopoulos and Bates [2021] to account for classifier uncertainty. Our empirical evaluation, conducted on nine graph classification datasets, provides evidence that our approach not only competes in performance with the baselines that use the complete graph information but also relies on significantly sparser subgraphs. Consequently, the resulting GNN-based predictions are more interpretable, addressing the primary motivation behind our work.

Practical limitations. The main limitation of our proposed approach lies in the significantly increased training and inference time, introduced by the reinforcement learning component, compared to the baselines that do not use reinforcement learning.

Future work. Future research could focus on improving the efficiency of the reinforcement learning component to accelerate the training process of CORES. Another interesting avenue for future work could involve modifying the current reward function to penalize specific types of errors or undesirable structures, such as isolated nodes. Additionally, it could also be interesting to explore the application of CORES to graph regression tasks and CORES_E to node classification tasks.

Acknowledgements

Pablo Sánchez Martín thanks the German Research Foundation through the Cluster of Excellence “Machine Learning – New Perspectives for Science”, EXC 2064/1, project number 390727645 for generous funding support. The authors thank the International Max Planck Research School for Intelligent Systems (IMPRS-IS) for supporting Pablo Sánchez Martín.

References

- Anastasios Nikolas Angelopoulos and Stephen Bates. A gentle introduction to conformal prediction and distribution-free uncertainty quantification. *ArXiv*, abs/2107.07511, 2021. URL <https://api.semanticscholar.org/CorpusID:235899036>.
- Anastasios Nikolas Angelopoulos, Stephen Bates, Jitendra Malik, and Michael I. Jordan. Uncertainty sets for image classifiers using conformal prediction. *ArXiv*, abs/2009.14193, 2020. URL <https://api.semanticscholar.org/CorpusID:221995507>.
- Ting Bai, Youjie Zhang, Bin Wu, and Jian-Yun Nie. Temporal graph neural networks for social recommendation. *2020 IEEE International Conference on Big Data (Big Data)*, pages 898–903, 2020.
- Karsten M. Borgwardt, Cheng Soon Ong, Stefan Schönauer, S. V. N. Vishwanathan, Alex Smola, and Hans-Peter Kriegel. Protein function prediction via graph kernels. *Bioinformatics*, 21 Suppl 1:i47–56, 2005.
- Shaked Brody, Uri Alon, and Eran Yahav. How attentive are graph attention networks? *ArXiv*, abs/2105.14491, 2021.

- Michael M. Bronstein, Joan Bruna, Yann LeCun, Arthur D. Szlam, and Pierre Vandergheynst. Geometric deep learning: Going beyond euclidean data. *IEEE Signal Processing Magazine*, 34:18–42, 2016.
- Cătălina Cangea, Petar Velickovic, Nikola Jovanovic, Thomas Kipf, and Pietro Lio'. Towards sparse hierarchical graph classifiers. *ArXiv*, abs/1811.01287, 2018. URL <https://api.semanticscholar.org/CorpusID:53219108>.
- Qi Cao, Huawei Shen, Jinhua Gao, Bingzheng Wei, and Xueqi Cheng. Coupled graph neural networks for predicting the popularity of online content. *ArXiv*, abs/1906.09032, 2019a.
- Qi Cao, Huawei Shen, Jinhua Gao, Bingzheng Wei, and Xueqi Cheng. Popularity prediction on social platforms with coupled graph neural networks. *Proceedings of the 13th International Conference on Web Search and Data Mining*, 2019b.
- Ming Chen, Zhewei Wei, Zengfeng Huang, Bolin Ding, and Yaliang Li. Simple and deep graph convolutional networks. In *International Conference on Machine Learning*, 2020.
- Martina Contisciani, Eleanor A. Power, and Caterina De Bacco. Community detection with node attributes in multilayer networks. *Scientific Reports*, 10, 2020.
- Gabriele Corso, Luca Cavalleri, D. Beaini, Pietro Lio', and Petar Velickovic. Principal neighbourhood aggregation for graph nets. *ArXiv*, abs/2004.05718, 2020.
- Asim Kumar Debnath, R L Lopez de Compadre, Gargi Debnath, Alan J. Shusterman, and Corwin Hansch. Structure-activity relationship of mutagenic aromatic and heteroaromatic nitro compounds. correlation with molecular orbital energies and hydrophobicity. *Journal of medicinal chemistry*, 34 2:786–97, 1991a.
- Asim Kumar Debnath, Rosa L. Lopez de Compadre, Gargi Debnath, Alan J. Shusterman, and Corwin Hansch. Structure-activity relationship of mutagenic aromatic and heteroaromatic nitro compounds. correlation with molecular orbital energies and hydrophobicity. *Journal of medicinal chemistry*, 34 2, 1991b. URL <https://api.semanticscholar.org/CorpusID:19990980>.
- Paul D. Dobson and Andrew J. Doig. Distinguishing enzyme structures from non-enzymes without alignments. *Journal of molecular biology*, 330 4:771–83, 2003.
- Finale Doshi-Velez and Been Kim. Towards a rigorous science of interpretable machine learning. *arXiv: Machine Learning*, 2017.
- Wenqi Fan, Yao Ma, Qing Li, Yuan He, Yihong Eric Zhao, Jiliang Tang, and Dawei Yin. Graph neural networks for social recommendation. *The World Wide Web Conference*, 2019.
- Matthias Fey and Jan E. Lenssen. Fast graph representation learning with PyTorch Geometric. In *ICLR Workshop on Representation Learning on Graphs and Manifolds*, 2019a.
- Matthias Fey and Jan E. Lenssen. Fast graph representation learning with PyTorch Geometric. In *ICLR Workshop on Representation Learning on Graphs and Manifolds*, 2019b.
- Hongyang Gao and Shuiwang Ji. Graph u-nets. *IEEE Transactions on Pattern Analysis and Machine Intelligence*, 44: 4948–4960, 2019.
- Justin Gilmer, Samuel S. Schoenholz, Patrick F. Riley, Oriol Vinyals, and George E. Dahl. Neural message passing for quantum chemistry. *ArXiv*, abs/1704.01212, 2017.
- Zhichun Guo, Chuxu Zhang, W. Yu, John E. Herr, O. Wiest, Meng Jiang, and N. Chawla. Few-shot graph learning for molecular property prediction. *Proceedings of the Web Conference 2021*, 2021.
- Arman Hasanzadeh, Ehsan Hajiramezani, Shahin Boluki, Mingyuan Zhou, Nick Duffield, Krishna Narayanan, and Xiaoning Qian. Bayesian graph neural networks with adaptive connection sampling. In *International conference on machine learning*, pages 4094–4104. PMLR, 2020.
- Adrián Javaloy, Pablo Sánchez-Martín, Amit Levi, and Isabel Valera. Learnable graph convolutional attention networks. *ArXiv*, abs/2211.11853, 2022.
- Thomas Kipf and Max Welling. Semi-supervised classification with graph convolutional networks. *ArXiv*, abs/1609.02907, 2016. URL <https://api.semanticscholar.org/CorpusID:3144218>.
- Boris Knyazev, Graham W. Taylor, and Mohamed R. Amer. Understanding attention and generalization in graph neural networks. In *Neural Information Processing Systems*, 2019. URL <https://api.semanticscholar.org/CorpusID:195069083>.
- Volodymyr Kuleshov and Doina Precup. Algorithms for multi-armed bandit problems. *arXiv preprint arXiv:1402.6028*, 2014.

- Junhyun Lee, Inyeop Lee, and Jaewoo Kang. Self-attention graph pooling. *ArXiv*, abs/1904.08082, 2019. URL <https://api.semanticscholar.org/CorpusID:119314157>.
- Jiayu Li, Tianyun Zhang, Hao Tian, Shengmin Jin, Makan Fardad, and Reza Zafarani. Sgcn: A graph sparsifier based on graph convolutional networks. In *Pacific-Asia Conference on Knowledge Discovery and Data Mining*, pages 275–287. Springer, 2020.
- Andreas Loukas. What graph neural networks cannot learn: depth vs width. *arXiv preprint arXiv:1907.03199*, 2019.
- Dongsheng Luo, Wei Cheng, Dongkuan Xu, Wenchao Yu, Bo Zong, Haifeng Chen, and Xiang Zhang. Parameterized explainer for graph neural network. *Advances in neural information processing systems*, 33:19620–19631, 2020.
- Dongsheng Luo, Wei Cheng, Wenchao Yu, Bo Zong, Jingchao Ni, Haifeng Chen, and Xiang Zhang. Learning to drop: Robust graph neural network via topological denoising. In *Proceedings of the 14th ACM International Conference on Web Search and Data Mining*, pages 779–787, 2021.
- Nina Mazyavkina, S. V. Sviridov, Sergei Ivanov, and Evgeny Burnaev. Reinforcement learning for combinatorial optimization: A survey. *Comput. Oper. Res.*, 134:105400, 2020. URL <https://api.semanticscholar.org/CorpusID:212633747>.
- Volodymyr Mnih, Koray Kavukcuoglu, David Silver, Andrei A. Rusu, Joel Veness, Marc G. Bellemare, Alex Graves, Martin A. Riedmiller, Andreas Kirkeby Fidjeland, Georg Ostrovski, Stig Petersen, Charlie Beattie, Amir Sadik, Ioannis Antonoglou, Helen King, Dhharshan Kumaran, Daan Wierstra, Shane Legg, and Demis Hassabis. Human-level control through deep reinforcement learning. *Nature*, 518:529–533, 2015.
- Mingshuo Nie, Dongming Chen, and Dongqi Wang. Reinforcement learning on graph: A survey. *ArXiv*, abs/2204.06127, 2022.
- Danilo Numeroso and Davide Bacciu. Meg: Generating molecular counterfactual explanations for deep graph networks. *arXiv preprint arXiv:2104.08060*, 2021.
- Kenta Oono and Taiji Suzuki. Graph neural networks exponentially lose expressive power for node classification. *arXiv preprint arXiv:1905.10947*, 2019.
- Ricardo Ramirez, Yu-Chiao Chiu, Allen Herrera, Milad Mostavi, Joshua Ramirez, Yidong Chen, Yufei Huang, and Yu-Fang Jin. Classification of cancer types using graph convolutional neural networks. In *Frontiers of Physics*, 2020.
- Yaniv Romano, Matteo Sesia, and Emmanuel J. Candès. Classification with valid and adaptive coverage. *arXiv: Methodology*, 2020. URL <https://api.semanticscholar.org/CorpusID:219303493>.
- Yu Rong, Wen bing Huang, Tingyang Xu, and Junzhou Huang. Dropedge: Towards deep graph convolutional networks on node classification. In *International Conference on Learning Representations*, 2019.
- Franco Scarselli, Marco Gori, Ah Chung Tsoi, Markus Hagenbuchner, and Gabriele Monfardini. The graph neural network model. *IEEE Transactions on Neural Networks*, 20:61–80, 2009.
- Michael Sejr Schlichtkrull, Nicola De Cao, and Ivan Titov. Interpreting graph neural networks for {nlp} with differentiable edge masking. In *International Conference on Learning Representations*, 2021. URL <https://openreview.net/forum?id=WznmQa42ZAx>.
- John Schulman, Filip Wolski, Prafulla Dhariwal, Alec Radford, and Oleg Klimov. Proximal policy optimization algorithms. *ArXiv*, abs/1707.06347, 2017a.
- John Schulman, Filip Wolski, Prafulla Dhariwal, Alec Radford, and Oleg Klimov. Proximal policy optimization algorithms. *arXiv preprint arXiv:1707.06347*, 2017b.
- Oleksandr Shchur and Stephan Günnemann. Overlapping community detection with graph neural networks. *ArXiv*, abs/1909.12201, 2018.
- Qingyun Sun, Jianxin Li, Hao Peng, Jia Wu, Yuanxing Ning, Philip S. Yu, and Lifang He. Sugar: Subgraph neural network with reinforcement pooling and self-supervised mutual information mechanism. In *Proceedings of the Web Conference 2021, WWW '21*, page 2081–2091, New York, NY, USA, 2021. Association for Computing Machinery. ISBN 9781450383127. doi: 10.1145/3442381.3449822. URL <https://doi.org/10.1145/3442381.3449822>.
- Richard S Sutton. Introduction: The challenge of reinforcement learning. *Reinforcement learning*, pages 1–3, 1992.
- Richard S. Sutton and Andrew G. Barto. Reinforcement learning: An introduction. *IEEE Transactions on Neural Networks*, 16:285–286, 2005.
- Richard S. Sutton, David A. McAllester, Satinder Singh, and Y. Mansour. Policy gradient methods for reinforcement learning with function approximation. In *NIPS*, 1999.

- Hannu (TT) Toivonen, Ashwin Srinivasan, Ross D. King, Stefan Kramer, and Christoph Helma. Statistical evaluation of the predictive toxicology challenge 2000-2001. *Bioinformatics*, 19 10:1183–93, 2003.
- Petar Velickovic, Guillem Cucurull, Arantxa Casanova, Adriana Romero, Pietro Lio', and Yoshua Bengio. Graph attention networks. *ArXiv*, abs/1710.10903, 2017.
- Nikil Wale, Ian A. Watson, and George Karypis. Comparison of descriptor spaces for chemical compound retrieval and classification. *Knowledge and Information Systems*, 14:347–375, 2006.
- Runzhong Wang, Zhigang Hua, Gan Liu, Jiayi Zhang, Junchi Yan, Feng Qi, Shuang Yang, Jun Zhou, and Xiaokang Yang. A bi-level framework for learning to solve combinatorial optimization on graphs. *arXiv preprint arXiv:2106.04927*, 2021.
- Ryan Wickman, Xiaofei Zhang, and Weizi Li. Sparrl: Graph sparsification via deep reinforcement learning. *arXiv preprint arXiv:2112.01565*, 2021.
- Shiwen Wu, Wentao Zhang, Fei Sun, and Bin Cui. Graph neural networks in recommender systems: A survey. *ACM Computing Surveys*, 55:1 – 37, 2020.
- Zonghan Wu, Shirui Pan, Fengwen Chen, Guodong Long, Chengqi Zhang, and Philip S. Yu. A comprehensive survey on graph neural networks. *IEEE Transactions on Neural Networks and Learning Systems*, 32:4–24, 2019.
- Zhaoping Xiong, Dingyan Wang, Xiaohong Liu, Feisheng Zhong, Xiaozhe Wan, Xutong Li, Zhaojun Li, Xiaomin Luo, Kaixian Chen, Hualiang Jiang, and Mingyue Zheng. Pushing the boundaries of molecular representation for drug discovery with graph attention mechanism. *Journal of medicinal chemistry*, 2020.
- Keyulu Xu, Weihua Hu, Jure Leskovec, and Stefanie Jegelka. How powerful are graph neural networks? *ArXiv*, abs/1810.00826, 2018.
- Rex Ying, Jiaxuan You, Christopher Morris, Xiang Ren, William L. Hamilton, and Jure Leskovec. Hierarchical graph representation learning with differentiable pooling. In *Neural Information Processing Systems*, 2018.
- Zhitao Ying, Dylan Bourgeois, Jiaxuan You, Marinka Zitnik, and Jure Leskovec. Gnnexplainer: Generating explanations for graph neural networks. *Advances in neural information processing systems*, 32, 2019.
- Zhaoning Yu and Hongyang Gao. Motifexplainer: a motif-based graph neural network explainer. *arXiv preprint arXiv:2202.00519*, 2022.
- Hao Yuan, Jiliang Tang, Xia Hu, and Shuiwang Ji. Xggn: Towards model-level explanations of graph neural networks. In *Proceedings of the 26th ACM SIGKDD International Conference on Knowledge Discovery & Data Mining*, pages 430–438, 2020.
- Hao Yuan, Haiyang Yu, Jie Wang, Kang Li, and Shuiwang Ji. On explainability of graph neural networks via subgraph explorations. In *Proceedings of the 38th International Conference on Machine Learning (ICML)*, pages 12241–12252, 2021.
- Cheng Zheng, Bo Zong, Wei Cheng, Dongjin Song, Jingchao Ni, Wenchao Yu, Haifeng Chen, and Wei Wang. Robust graph representation learning via neural sparsification. In *International Conference on Machine Learning*, pages 11458–11468. PMLR, 2020.
- Liyuan Zheng, Tanner Fiez, Zane Alumbaugh, Benjamin J. Chasnov, and Lillian J. Ratliff. Stackelberg actor-critic: Game-theoretic reinforcement learning algorithms. *ArXiv*, abs/2109.12286, 2021.

Table 4: **Best configuration for the Vanilla GNN.** Split sizes (#0), Batch size (#1), Dropout rate (#2), Batch normalizing (#3), Dimension of hidden layers (#4), Number of GNN layers (#5), Global pooling type (#6), Classifier scheduler factor (#7), Classifier learning rate (#8), ϵ (#9), Trainable ϵ (#10), Number of heads (#11).

Param	Archi	Datasets								
		BZR	COX2	DD	ENZYMES	MUTAG	NCII	NCII09	PROTEINS	PTC
#0	GIN	[0.6, 0.3, 0.1]	[0.4, 0.5, 0.1]	[0.6, 0.3, 0.1]	[0.5, 0.4, 0.1]	[0.4, 0.5, 0.1]	[0.5, 0.4, 0.1]	[0.4, 0.5, 0.1]	[0.4, 0.5, 0.1]	[0.6, 0.3, 0.1]
	GAT	[0.6, 0.3, 0.1]	[0.5, 0.4, 0.1]	[0.5, 0.4, 0.1]	[0.5, 0.4, 0.1]	[0.5, 0.4, 0.1]	[0.6, 0.3, 0.1]	[0.6, 0.3, 0.1]	[0.4, 0.5, 0.1]	[0.5, 0.4, 0.1]
	GCN	[0.6, 0.3, 0.1]	[0.5, 0.4, 0.1]	[0.6, 0.3, 0.1]	[0.5, 0.4, 0.1]	[0.5, 0.4, 0.1]	[0.6, 0.3, 0.1]	[0.6, 0.3, 0.1]	[0.4, 0.5, 0.1]	[0.4, 0.5, 0.1]
#1	GIN	16	16	32	16	16	16	32	16	32
	GAT	32	16	32	16	16	32	32	16	16
	GCN	16	16	32	16	32	32	16	32	32
#2	GIN	0.0	0.2	0.5	0.2	0.0	0.0	0.1	0.1	0.4
	GAT	0.1	0.2	0.3	0.4	0.3	0.2	0.1	0.1	0.5
	GCN	0.3	0.1	0.3	0.0	0.4	0.0	0.1	0.4	0.5
#3	GIN	True	False	True	True	True	True	True	False	False
	GAT	True	True	False	True	True	True	False	True	True
	GCN	True	False	False	True	False	True	True	False	False
#4	GIN	128	64	32	64	16	128	128	128	16
	GAT	16	128	16	128	32	128	128	16	16
	GCN	64	128	32	128	16	64	128	32	32
#5	GIN	3	1	1	1	3	1	3	1	3
	GAT	1	2	1	4	4	4	3	2	4
	GCN	1	4	3	3	4	3	4	1	1
#6	GIN	['mean', 'add']	['add']	['mean', 'add']	['mean']	['mean', 'add']	['mean']	['mean']	['add']	['mean']
	GAT	['add']	['mean']	['mean', 'add']	['mean']	['mean', 'add']	['add']	['mean', 'add']	['add']	['mean', 'add']
	GCN	['mean']	['mean', 'add']	['mean', 'add']	['mean']	['mean', 'add']	['mean', 'add']	['add']	['add']	['mean']
#7	GIN	0.95	0.99	0.99	0.9	0.95	0.9	0.99	0.9	0.99
	GAT	0.95	0.95	0.99	0.95	0.99	0.95	0.99	0.95	0.9
	GCN	0.99	0.99	0.99	0.95	0.99	0.99	0.9	0.99	0.99
#8	GIN	0.0001	0.001	0.005	0.0001	0.001	0.01	0.001	0.0005	0.005
	GAT	0.01	0.0001	0.0001	0.001	0.005	0.005	0.001	0.005	0.01
	GCN	0.01	0.0001	0.001	0.01	0.005	0.005	0.001	0.001	0.01
#9	GIN	0.3	0.2	0.3	0.0	0.2	0.2	0.2	0.0	0.2
	GAT	-	-	-	-	-	-	-	-	-
	GCN	-	-	-	-	-	-	-	-	-
#10	GIN	False	True	True	True	True	False	True	False	False
	GAT	-	-	-	-	-	-	-	-	-
	GCN	-	-	-	-	-	-	-	-	-
#11	GIN	-	-	-	-	-	-	-	-	-
	GAT	2.0	4.0	4.0	2.0	2.0	4.0	4.0	2.0	4.0
	GCN	-	-	-	-	-	-	-	-	-

A Training details

In this section, we provide further details of the experimental setup used to obtain our results. For all experiments, we train the models using a fixed seed of 0, and the reported results represent the mean and standard deviation over five different dataset splits. We run the models up to 1000 epochs, doing early stopping if the accuracy does not improve for 500 epochs. All experiments were conducted on a single CPU with 8GB of RAM. We carry out hyperparameter tuning using random sampling. We explored 20 different configurations for each model, data, and GNN architecture. Complete details regarding the cross-validated hyperparameters can be found in our GitHub repository at <https://github.com/psanch21/CORES>. Table 4 presents the best configurations achieved for each dataset and architecture for the Vanilla GNN baselines. These configurations were subsequently used for training CORES. The best configuration for CORES_N is detailed in Table 7, while for CORES_E, it can be found in Table 8. The best configurations for SAGPooling and GPool are outlined in Table 5 and Table 6, respectively.

Table 5: **Best configuration for SAGPooling.** Split sizes (#0), Batch size (#1), Early stopping clf. patience (#2), Dropout rate (#3), Batch normalizing (#4), Dimension of hidden layers (#5), Number of GNN layers (#6), Global pooling type (#7), Classifier scheduler factor (#8), Classifier learning rate (#9), TopK multiplier (#10), TopK ratio (#11), Number of heads (#12), ϵ (#13), Trainable ϵ (#14)

Param	Archi	Datasets								
		BZR	COX2	DD	ENZYMES	MUTAG	NCI1	NCI109	PROTEINS	PTC
#0	GCN	[0.5, 0.4, 0.1]	[0.5, 0.4, 0.1]	[0.4, 0.5, 0.1]	[0.5, 0.4, 0.1]	[0.5, 0.4, 0.1]	[0.5, 0.4, 0.1]	[0.5, 0.4, 0.1]	[0.4, 0.5, 0.1]	[0.6, 0.3, 0.1]
	GAT	[0.4, 0.5, 0.1]	[0.4, 0.5, 0.1]	[0.4, 0.5, 0.1]	[0.5, 0.4, 0.1]	[0.4, 0.5, 0.1]	[0.6, 0.3, 0.1]	[0.5, 0.4, 0.1]	[0.4, 0.5, 0.1]	[0.4, 0.5, 0.1]
	GIN	[0.5, 0.4, 0.1]	[0.5, 0.4, 0.1]	[0.5, 0.4, 0.1]	[0.6, 0.3, 0.1]	[0.5, 0.4, 0.1]	[0.5, 0.4, 0.1]	[0.6, 0.3, 0.1]	[0.6, 0.3, 0.1]	[0.5, 0.4, 0.1]
#1	GCN	16	16	16	16	32	16	16	16	32
	GAT	16	16	16	16	16	16	32	16	16
	GIN	16	16	16	32	32	16	32	32	16
#2	GCN	800	650	500	650	500	650	650	500	650
	GAT	800	800	500	800	800	650	500	800	800
	GIN	800	500	650	500	800	800	500	500	650
#3	GCN	0.4	0.0	0.5	0.1	0.4	0.0	0.1	0.5	0.4
	GAT	0.3	0.3	0.1	0.1	0.4	0.1	0.4	0.3	0.3
	GIN	0.2	0.3	0.5	0.0	0.4	0.2	0.0	0.0	0.5
#4	GCN	True	False	False	True	True	False	True	False	False
	GAT	False	False	False	False	True	True	False	False	False
	GIN	True	False	False	True	False	True	True	True	False
#5	GCN	128	32	32	128	32	32	128	32	64
	GAT	16	16	64	128	16	32	16	16	16
	GIN	32	128	128	64	16	32	64	64	128
#6	GCN	4	1	4	4	1	1	4	4	3
	GAT	1	1	2	2	2	3	2	1	1
	GIN	4	4	3	1	2	4	1	1	3
#7	GCN	['add']	['mean', 'add']	['add']	['mean']	['mean', 'add']	['mean', 'add']	['mean']	['add']	['mean']
	GAT	['mean', 'add']	['mean', 'add']	['mean', 'add']	['mean', 'add']	['mean', 'add']	['mean']	['mean', 'add']	['mean', 'add']	['mean', 'add']
	GIN	['mean']	['mean']	['mean']	['add']	['mean', 'add']	['mean']	['add']	['add']	['mean']
#8	GCN	0.99	0.95	0.99	0.95	0.9	0.95	0.95	0.99	0.9
	GAT	0.9	0.9	0.9	0.99	0.99	0.95	0.99	0.9	0.9
	GIN	0.9	0.99	0.95	0.95	0.99	0.9	0.95	0.95	0.95
#9	GCN	0.01	0.005	0.0005	0.0001	0.01	0.005	0.0001	0.0005	0.0001
	GAT	0.01	0.01	0.01	0.005	0.005	0.0001	0.005	0.01	0.01
	GIN	0.001	0.0005	0.0005	0.001	0.005	0.001	0.001	0.001	0.0005
#10	GCN	0.5	2.0	0.5	1.5	1.0	2.0	1.5	0.5	0.5
	GAT	1.0	1.0	2.0	1.0	1.5	1.5	0.5	1.0	1.0
	GIN	1.5	2.0	0.5	0.5	0.5	1.5	0.5	0.5	0.5
#11	GCN	0.95	0.95	0.9	0.3	0.3	0.95	0.3	0.9	0.2
	GAT	0.9	0.9	0.5	0.9	0.2	0.6	0.8	0.9	0.9
	GIN	0.3	0.4	0.8	0.3	0.8	0.3	0.3	0.3	0.8
#12	GCN	-	-	-	-	-	-	-	-	-
	GAT	1.0	1.0	1.0	1.0	1.0	1.0	4.0	1.0	1.0
	GIN	-	-	-	-	-	-	-	-	-
#13	GCN	-	-	-	-	-	-	-	-	-
	GAT	-	-	-	-	-	-	-	-	-
	GIN	0.4	0.2	0.4	0.4	0.3	0.4	0.4	0.4	0.4
#14	GCN	-	-	-	-	-	-	-	-	-
	GAT	-	-	-	-	-	-	-	-	-
	GIN	False	True	True	True	False	False	True	True	True

Table 6: **Best configuration for the GPool.** Split sizes (#0), Batch size (#1), Early stopping clf. patience (#2), Dropout rate (#3), Batch normalizing (#4), Dimension of hidden layers (#5), Number of GNN layers (#6), Global pooling type (#7), Classifier scheduler factor (#8), Classifier learning rate (#9), TopK multiplier (#10), TopK ratio (#11), Number of heads (#12), ϵ (#13), Trainable ϵ (#14).

Param	Archi	Datasets								
		BZR	COX2	DD	ENZYMES	MUTAG	NCI1	NCI109	PROTEINS	PTC
#0	GAT	[0.5, 0.4, 0.1]	[0.6, 0.3, 0.1]	[0.6, 0.3, 0.1]	[0.4, 0.5, 0.1]	[0.4, 0.5, 0.1]	[0.4, 0.5, 0.1]	[0.4, 0.5, 0.1]	[0.4, 0.5, 0.1]	[0.4, 0.5, 0.1]
	GIN	[0.4, 0.5, 0.1]	[0.4, 0.5, 0.1]	[0.4, 0.5, 0.1]	[0.4, 0.5, 0.1]	[0.5, 0.4, 0.1]	[0.4, 0.5, 0.1]	[0.4, 0.5, 0.1]	[0.4, 0.5, 0.1]	[0.5, 0.4, 0.1]
	GCN	[0.4, 0.5, 0.1]	[0.4, 0.5, 0.1]	[0.4, 0.5, 0.1]	[0.4, 0.5, 0.1]	[0.5, 0.4, 0.1]	[0.4, 0.5, 0.1]	[0.4, 0.5, 0.1]	[0.4, 0.5, 0.1]	[0.6, 0.3, 0.1]
#1	GAT	16	16	16	32	32	32	32	32	32
	GIN	32	16	16	32	16	32	32	16	32
	GCN	16	16	32	32	16	32	32	32	16
#2	GAT	500	650	800	500	500	500	500	650	800
	GIN	500	800	800	500	800	500	500	800	800
	GCN	650	650	500	500	650	500	500	800	650
#3	GAT	0.0	0.3	0.5	0.1	0.1	0.1	0.1	0.1	0.3
	GIN	0.1	0.0	0.5	0.1	0.4	0.1	0.1	0.5	0.2
	GCN	0.0	0.0	0.4	0.1	0.0	0.3	0.1	0.5	0.1
#4	GAT	True	True	False	True	True	True	True	False	False
	GIN	True	True	False	True	False	True	True	False	False
	GCN	True	True	False	True	True	True	True	True	False
#5	GAT	16	64	16	64	64	64	64	16	64
	GIN	64	32	16	64	32	64	64	16	128
	GCN	128	128	128	64	32	128	64	16	16
#6	GAT	2	4	1	2	2	2	2	1	3
	GIN	2	1	1	2	1	2	2	1	4
	GCN	2	2	2	2	4	3	2	3	3
#7	GAT	['mean', 'add']	['mean']	['mean', 'add']	['mean']	['mean']	['mean']	['mean']	['add']	['add']
	GIN	['mean']	['mean']	['mean', 'add']	['mean']	['mean', 'add']	['mean']	['mean']	['mean', 'add']	['add']
	GCN	['mean']	['mean']	['add']	['mean']	['mean', 'add']	['mean', 'add']	['mean']	['mean', 'add']	['mean']
#8	GAT	0.9	0.95	0.9	0.9	0.9	0.9	0.9	0.95	0.99
	GIN	0.9	0.9	0.9	0.9	0.9	0.9	0.9	0.9	0.9
	GCN	0.95	0.95	0.99	0.9	0.99	0.9	0.9	0.99	0.95
#9	GAT	0.005	0.0005	0.001	0.01	0.01	0.01	0.01	0.001	0.0005
	GIN	0.01	0.0001	0.001	0.01	0.01	0.01	0.01	0.001	0.0001
	GCN	0.0001	0.0001	0.01	0.01	0.01	0.001	0.01	0.001	0.005
#10	GAT	2.0	0.5	1.5	2.0	2.0	2.0	2.0	1.5	0.5
	GIN	2.0	2.0	1.5	2.0	1.0	2.0	2.0	1.5	0.5
	GCN	1.0	1.0	1.5	2.0	0.5	1.0	2.0	0.5	1.5
#11	GAT	0.4	0.5	0.4	0.95	0.95	0.95	0.95	0.5	0.5
	GIN	0.95	0.9	0.4	0.95	0.5	0.95	0.95	0.4	0.4
	GCN	0.95	0.95	0.4	0.95	0.7	0.95	0.95	0.5	0.8
#12	GAT	4.0	1.0	1.0	1.0	1.0	1.0	1.0	1.0	1.0
	GIN	-	-	-	-	-	-	-	-	-
	GCN	-	-	-	-	-	-	-	-	-
#13	GAT	-	-	-	-	-	-	-	-	-
	GIN	0.0	0.4	0.1	0.0	0.1	0.0	0.0	0.1	0.2
	GCN	-	-	-	-	-	-	-	-	-
#14	GAT	-	-	-	-	-	-	-	-	-
	GIN	True	True	False	True	True	True	True	False	True
	GCN	-	-	-	-	-	-	-	-	-

Table 7: **Best configuration for CORES_N**. Early stopping PPO patience (#0), Number of environment steps (#1), Number of PPO epochs (#2), Environment penalty size (#3), RL scheduler factor (#4), Ratio of the critic learning rate (#5), PPO entropy coefficient (#6), PPO MSE coefficient (#7), PPO clip value ϵ (#8), Conformal error rate α (#9), d (#10), λ (#11).

Param	Archi	Datasets								
		BZR	COX2	DD	ENZYMES	MUTAG	NCI1	NCI109	PROTEINS	PTC
#0	GIN	15	5	5	10	10	5	15	5	5
	GCN	10	5	5	15	5	15	10	15	15
	GAT	15	5	5	10	15	15	10	10	5
#1	GIN	128	128	128	128	128	128	64	64	64
	GCN	32	64	64	128	64	32	32	32	128
	GAT	64	32	32	32	128	64	32	32	64
#2	GIN	10	15	15	5	15	15	10	5	15
	GCN	10	15	15	5	15	3	10	5	5
	GAT	10	15	15	10	5	10	10	5	5
#3	GIN	0.5	0.5	0.5	0.5	0.5	0.5	1.5	1.5	1.0
	GCN	0.5	0.5	0.5	1.0	0.5	0.5	0.5	1.5	1.5
	GAT	1.5	0.5	1.5	0.5	1.5	1.5	0.5	1.0	1.5
#4	GIN	0.99	0.95	0.95	0.99	0.9	0.95	0.9	0.9	0.95
	GCN	0.99	0.95	0.95	0.99	0.95	0.99	0.99	0.9	0.9
	GAT	0.9	0.95	0.99	0.99	0.9	0.9	0.99	0.95	0.9
#5	GIN	3.0	2.5	2.5	1.0	3.0	2.5	2.5	1.0	3.0
	GCN	2.5	1.5	1.5	2.0	1.5	3.0	2.5	2.5	1.5
	GAT	2.5	2.0	2.5	2.5	1.5	2.5	2.5	1.0	1.0
#6	GIN	0.001	0.0001	0.0001	0.01	0.001	0.0001	0.0001	0.001	0.0001
	GCN	0.0001	0.01	0.01	0.0001	0.01	0.01	0.0001	0.01	0.001
	GAT	0.0001	0.001	0.001	0.0001	0.001	0.0001	0.0001	0.001	0.001
#7	GIN	0.5	5.0	5.0	2.0	1.0	5.0	2.0	3.0	0.5
	GCN	1.0	0.5	0.5	0.1	0.5	1.0	1.0	5.0	3.0
	GAT	2.0	1.0	3.0	1.0	3.0	2.0	1.0	0.1	3.0
#8	GIN	0.2	0.4	0.4	0.1	0.2	0.4	0.2	0.1	0.4
	GCN	0.4	0.3	0.3	0.3	0.3	0.1	0.4	0.3	0.1
	GAT	0.2	0.2	0.4	0.4	0.1	0.2	0.4	0.4	0.1
#9	GIN	0.2	0.05	0.05	0.1	0.2	0.05	0.2	0.05	0.05
	GCN	0.05	0.2	0.2	0.05	0.2	0.1	0.05	0.2	0.05
	GAT	0.2	0.2	0.2	0.05	0.05	0.2	0.05	0.05	0.05
#10	GIN	0.2	0.3	0.3	0.7	0.7	0.3	0.4	0.2	0.5
	GCN	0.9	0.8	0.8	0.6	0.8	0.4	0.9	0.5	0.2
	GAT	0.4	0.6	0.6	0.9	0.2	0.4	0.9	0.6	0.2
#11	GIN	0.2	1.0	1.0	0.9	0.1	1.0	0.4	0.0	0.4
	GCN	0.2	0.7	0.7	1.0	0.7	0.8	0.2	0.8	0.7
	GAT	0.4	0.3	0.8	0.2	0.7	0.4	0.2	0.5	0.0

Table 8: **Best configuration for CORES_E**. Early stopping PPO patience (#0), Number of environment steps (#1), Number of PPO epochs (#2), Environment penalty size (#3), RL scheduler factor (#4), Ratio of the critic learning rate (#5), PPO entropy coefficient (#6), PPO MSE coefficient (#7), PPO clip value ϵ (#8), Conformal error rate α (#9), d (#10), λ (#11).

Param	Archi	Datasets								
		BZR	COX2	DD	ENZYMES	MUTAG	NCI1	NCI109	PROTEINS	PTC
#0	GIN	15	5	5	10	10	5	15	5	5
	GCN	10	5	5	15	5	15	10	15	15
	GAT	15	5	5	10	15	15	10	10	5
#1	GIN	128	128	128	128	128	128	64	64	64
	GCN	32	64	64	128	64	32	32	32	128
	GAT	64	32	32	32	128	64	32	32	64
#2	GIN	10	15	15	5	15	15	10	5	15
	GCN	10	15	15	5	15	3	10	5	5
	GAT	10	15	15	10	5	10	10	5	5
#3	GIN	0.5	0.5	0.5	0.5	0.5	0.5	1.5	1.5	1.0
	GCN	0.5	0.5	0.5	1.0	0.5	0.5	0.5	1.5	1.5
	GAT	1.5	0.5	1.5	0.5	1.5	1.5	0.5	1.0	1.5
#4	GIN	0.99	0.95	0.95	0.99	0.9	0.95	0.9	0.9	0.95
	GCN	0.99	0.95	0.95	0.99	0.95	0.99	0.99	0.9	0.9
	GAT	0.9	0.95	0.99	0.99	0.9	0.9	0.99	0.95	0.9
#5	GIN	3.0	2.5	2.5	1.0	3.0	2.5	2.5	1.0	3.0
	GCN	2.5	1.5	1.5	2.0	1.5	3.0	2.5	2.5	1.5
	GAT	2.5	2.0	2.5	2.5	1.5	2.5	2.5	1.0	1.0
#6	GIN	0.001	0.0001	0.0001	0.01	0.001	0.0001	0.0001	0.001	0.0001
	GCN	0.0001	0.01	0.01	0.0001	0.01	0.01	0.0001	0.01	0.001
	GAT	0.0001	0.001	0.001	0.0001	0.001	0.0001	0.0001	0.001	0.001
#7	GIN	0.5	5.0	5.0	2.0	1.0	5.0	2.0	3.0	0.5
	GCN	1.0	0.5	0.5	0.1	0.5	1.0	1.0	5.0	3.0
	GAT	2.0	1.0	3.0	1.0	3.0	2.0	1.0	0.1	3.0
#8	GIN	0.2	0.4	0.4	0.1	0.2	0.4	0.2	0.1	0.4
	GCN	0.4	0.3	0.3	0.3	0.3	0.1	0.4	0.3	0.1
	GAT	0.2	0.2	0.4	0.4	0.1	0.2	0.4	0.4	0.1
#9	GIN	0.2	0.05	0.05	0.1	0.2	0.05	0.2	0.05	0.05
	GCN	0.05	0.2	0.2	0.05	0.2	0.1	0.05	0.2	0.05
	GAT	0.2	0.2	0.2	0.05	0.05	0.2	0.05	0.05	0.05
#10	GIN	0.2	0.3	0.3	0.7	0.7	0.3	0.4	0.2	0.5
	GCN	0.9	0.8	0.8	0.6	0.8	0.4	0.9	0.5	0.2
	GAT	0.4	0.6	0.6	0.9	0.2	0.4	0.9	0.6	0.2
#11	GIN	0.2	1.0	1.0	0.9	0.1	1.0	0.4	0.0	0.4
	GCN	0.2	0.7	0.7	1.0	0.7	0.8	0.2	0.8	0.7
	GAT	0.4	0.3	0.8	0.2	0.7	0.4	0.2	0.5	0.0

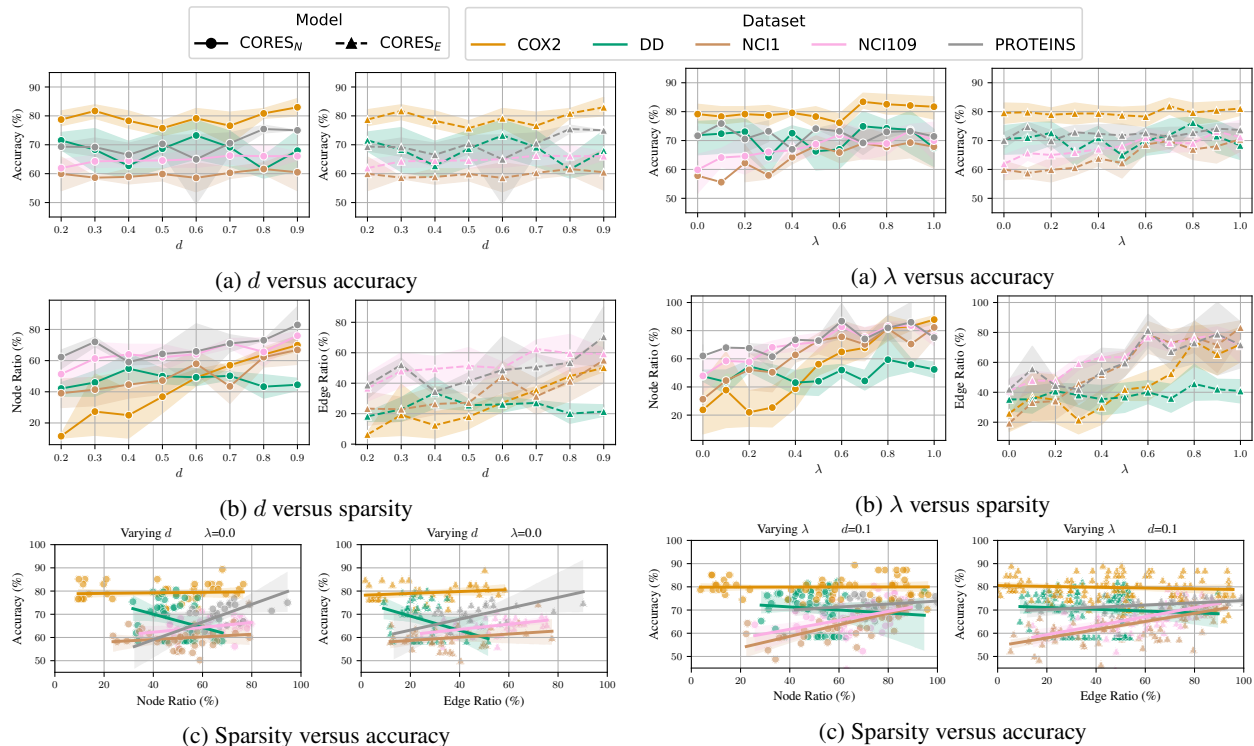


Figure 6: Ablation study on the maximum desired ratio d for 5 different runs for the GIN architecture.

Figure 7: Ablation study on λ for 5 different runs for the GIN architecture.

B Extra results impact of hyperparameters

In this section, we present an ablation study on the impact of two key hyperparameters of CORES, namely d and λ , for the datasets not included in the main manuscript: COX2, DD, NCI1, NCI109, and PROTEINS. Figure 6 illustrates the results of the ablation study for parameter d , while the results for parameter λ are shown in Figure 7.

The findings from this ablation study are consistent with those reported in the main manuscript. In the top row figures, we observe that the accuracy remains relatively stable when varying either d or λ , improving only as the values increase for certain datasets, such as NCI1 or NCI109. In the middle row figures, we find a positive correlation between both parameters and the node/edge ratio for most of the datasets, and no correlation for others. Remarkably, the correlation is never negative. Finally, the bottom row figures reveal a positive correlation between the node/edge ratio and accuracy for the majority of the datasets. This pattern holds except for the DD dataset, which presents a negative correlation. Interestingly this dataset presents the most significant disparities in terms of the number of nodes and edges compared to the other datasets (see Table 1).

Table 9: **Model comparison results with GAT architecture.** We show the mean over 5 independent runs and the standard deviation as the subindex. All metrics are shown in percentage. The last rows include the average ranking of the model across datasets.

Dataset	Metric	Models				
		GNN	SAGPool	GPool	CORES _N	CORES _E
BZR	Accuracy	80.98 _{4.36}	83.90 _{3.27}	79.51 _{6.12}	83.90 _{4.43}	81.46 _{4.08}
	Node Ratio	-	-	41.11 _{0.11}	37.99 _{10.27}	100.00 _{0.00}
	Edge Ratio	-	-	20.93 _{0.70}	29.92 _{8.83}	57.26 _{21.50}
COX2	Accuracy	82.13 _{4.15}	80.00 _{4.41}	77.87 _{3.87}	81.70 _{4.41}	80.85 _{2.61}
	Node Ratio	-	-	50.62 _{0.09}	77.91 _{2.29}	100.00 _{0.00}
	Edge Ratio	-	-	20.75 _{0.51}	62.62 _{3.24}	66.18 _{0.38}
DD	Accuracy	76.10 _{3.02}	75.76 _{3.72}	77.80 _{1.84}	75.42 _{4.19}	76.44 _{2.19}
	Node Ratio	-	-	40.24 _{0.03}	75.16 _{1.39}	100.00 _{0.00}
	Edge Ratio	-	-	15.63 _{0.29}	56.42 _{2.16}	58.62 _{2.51}
ENZYMES	Accuracy	71.33 _{10.63}	45.00 _{7.64}	63.93 _{6.35}	69.84 _{4.43}	67.54 _{12.23}
	Node Ratio	-	-	96.67 _{0.14}	80.26 _{1.03}	100.00 _{0.00}
	Edge Ratio	-	-	93.27 _{0.23}	65.92 _{1.80}	61.60 _{9.06}
MUTAG	Accuracy	81.43 _{6.39}	88.57 _{3.91}	78.57 _{7.14}	80.00 _{5.98}	81.43 _{6.02}
	Node Ratio	-	-	97.81 _{0.36}	75.72 _{4.04}	100.00 _{0.00}
	Edge Ratio	-	-	95.65 _{2.50}	58.74 _{6.05}	55.25 _{14.77}
NCI1	Accuracy	79.42 _{1.34}	68.93 _{1.37}	72.43 _{2.11}	73.43 _{2.67}	75.38 _{1.22}
	Node Ratio	-	-	96.89 _{0.08}	63.49 _{3.58}	100.00 _{0.00}
	Edge Ratio	-	-	94.07 _{0.34}	53.33 _{2.81}	88.68 _{6.67}
NCI109	Accuracy	76.90 _{1.34}	67.46 _{4.31}	67.22 _{3.25}	74.72 _{2.25}	72.78 _{2.29}
	Node Ratio	-	-	96.79 _{0.04}	71.55 _{11.30}	100.00 _{0.00}
	Edge Ratio	-	-	94.70 _{0.98}	62.37 _{12.96}	61.37 _{13.13}
PROTEINS	Accuracy	75.36 _{3.00}	72.68 _{3.26}	73.21 _{3.22}	73.39 _{3.86}	73.57 _{1.62}
	Node Ratio	-	-	51.15 _{0.17}	67.94 _{2.97}	100.00 _{0.00}
	Edge Ratio	-	-	28.39 _{0.42}	46.56 _{4.27}	52.82 _{1.86}
PTC	Accuracy	64.00 _{4.33}	65.00 _{6.39}	62.44 _{4.12}	62.96 _{4.17}	59.43 _{4.69}
	Node Ratio	-	-	52.46 _{0.41}	45.61 _{6.00}	100.00 _{0.00}
	Edge Ratio	-	-	36.58 _{3.53}	21.24 _{6.53}	76.36 _{14.75}
Avg. Rank	Accuracy	1.89	3.33	3.89	3.00	2.89
	Node Ratio	-	-	1.67	1.33	-
	Edge Ratio	-	-	2.33	1.56	2.11

C Extra comparison results

Here, we analyze the results of how switching the base model affects the performance. Table 10 and Table 9 summarizes the results for two base architectures GCN and GAT. It can be observed that even when the base architecture changes our models CORES_N and CORES_E achieve competitive accuracy compared to the respective baseline and achieve top rankings in terms of node/edge ratio.

Table 10: **Model comparison results with GCN architecture** We show the mean over 5 independent runs and the standard deviation as the subindex. All metrics are shown in percentage. The last rows include the average ranking of the model across datasets.

Dataset	Metric	Models				
		GNN	SAGPool	GPool	CORES _N	CORES _E
BZR	Accuracy	86.83 _{4.08}	83.41 _{4.69}	84.39 _{4.08}	82.44 _{4.69}	80.98 _{5.29}
	Node Ratio	-	-	96.46 _{0.19}	76.98 _{6.06}	100.00 _{0.00}
	Edge Ratio	-	-	92.87 _{0.58}	61.17 _{11.31}	46.16 _{5.68}
COX2	Accuracy	79.15 _{4.85}	80.43 _{3.81}	80.00 _{1.90}	80.85 _{3.01}	81.70 _{4.90}
	Node Ratio	-	-	96.14 _{0.18}	72.49 _{4.24}	100.00 _{0.00}
	Edge Ratio	-	-	92.67 _{0.71}	53.19 _{8.07}	31.27 _{23.60}
DD	Accuracy	78.47 _{3.47}	75.93 _{4.39}	76.10 _{5.06}	79.32 _{2.58}	75.76 _{4.05}
	Node Ratio	-	-	40.23 _{0.03}	56.44 _{2.50}	100.00 _{0.00}
	Edge Ratio	-	-	16.48 _{0.13}	32.01 _{2.89}	51.39 _{1.90}
ENZYMES	Accuracy	66.00 _{5.35}	52.00 _{5.70}	64.59 _{4.86}	58.31 _{8.47}	57.02 _{11.62}
	Node Ratio	-	-	96.67 _{0.14}	77.17 _{7.28}	100.00 _{0.00}
	Edge Ratio	-	-	93.39 _{0.35}	62.33 _{9.26}	74.20 _{35.99}
MUTAG	Accuracy	81.43 _{3.91}	80.00 _{3.19}	78.57 _{5.05}	81.43 _{10.83}	87.14 _{6.56}
	Node Ratio	-	-	73.13 _{0.55}	79.94 _{2.79}	100.00 _{0.00}
	Edge Ratio	-	-	68.22 _{2.47}	63.52 _{4.23}	32.66 _{8.79}
NCI1	Accuracy	77.33 _{2.09}	73.58 _{1.64}	72.14 _{2.64}	66.45 _{7.71}	65.94 _{6.31}
	Node Ratio	-	-	96.89 _{0.08}	76.47 _{17.88}	100.00 _{0.00}
	Edge Ratio	-	-	96.06 _{0.20}	64.02 _{18.84}	37.98 _{14.34}
NCI109	Accuracy	79.32 _{1.57}	71.19 _{2.03}	71.53 _{2.12}	76.08 _{2.71}	77.14 _{2.02}
	Node Ratio	-	-	96.79 _{0.04}	78.78 _{4.15}	100.00 _{0.00}
	Edge Ratio	-	-	95.82 _{0.11}	67.08 _{4.42}	92.02 _{1.93}
PROTEINS	Accuracy	72.86 _{1.02}	72.86 _{3.13}	75.18 _{2.75}	73.21 _{2.45}	75.89 _{1.94}
	Node Ratio	-	-	51.15 _{0.17}	74.66 _{6.10}	100.00 _{0.00}
	Edge Ratio	-	-	28.15 _{0.67}	56.12 _{9.77}	64.73 _{0.98}
PTC	Accuracy	57.78 _{7.71}	64.57 _{3.83}	63.43 _{1.28}	62.86 _{2.86}	63.43 _{3.13}
	Node Ratio	-	-	83.80 _{0.74}	64.10 _{4.19}	100.00 _{0.00}
	Edge Ratio	-	-	78.21 _{3.76}	40.21 _{6.93}	44.47 _{5.29}
Avg. Rank	Accuracy	1.89	3.33	3.89	3.00	2.89
	Node Ratio	-	-	1.67	1.33	-
	Edge Ratio	-	-	2.56	1.67	1.78

Table 11: **Training time comparison.** We show the average training time in seconds along with the standard deviation of each model on each dataset for one epoch with a batch size of one. We use the GIN GNN architecture.

Dataset	Full Models		Sparse Models			
	Vanilla	DiffPool	SUGAR	GPool	CORES _N	CORES _E
BZR	2.64 _{0.18}	4.23 _{0.12}	-	3.44 _{0.27}	186.96 _{61.70}	121.94 _{2.00}
COX2	3.07 _{0.15}	4.83 _{0.17}	-	10.00 _{2.70}	411.93 _{85.97}	203.93 _{1.86}
DD	6.13 _{0.13}	-	-	33.31 _{4.90}	1848.21 _{1.12}	1857.59 _{1.13}
ENZYMES	2.40 _{0.04}	6.26 _{0.31}	132.86 _{3.77}	6.08 _{0.30}	233.78 _{6.65}	287.95 _{2.20}
MUTAG	1.09 _{0.03}	1.63 _{0.04}	47.82 _{3.45}	1.71 _{0.19}	24.97 _{1.55}	22.94 _{0.30}
NCI1	15.44 _{0.19}	41.74 _{3.03}	1143.85 _{45.27}	48.05 _{8.12}	1596.95 _{107.83}	1826.41 _{51.06}
NCI109	16.68 _{1.15}	43.73 _{0.44}	1195.10 _{47.42}	43.46 _{3.09}	1533.59 _{15.51}	1756.84 _{37.12}
PROTEINS	5.80 _{0.23}	11.79 _{1.19}	511.21 _{22.63}	13.58 _{2.58}	484.97 _{14.74}	505.89 _{2.70}
PTC	1.68 _{0.16}	3.00 _{0.07}	95.78 _{1.47}	3.28 _{0.18}	64.60 _{1.23}	67.19 _{0.32}

D Time complexity

We analyze the training and inference times of all models on each dataset. We run each model on every dataset for a single epoch, utilizing a batch size of one. To ensure statistical significance and reliability in our measurements, we repeat each experiment ten times. This repetition enables us to calculate the average training and inference times accurately. Such a meticulous approach guarantees robust and precise performance assessment for our models across the diverse set of datasets under examination.

Table 11 and Table 12 show the complete results for the training and inferences times, respectively. If we focus on Table 11, we observe the models that only rely on a single forward pass are two orders of magnitude faster than the models that rely on a reinforcement learning-based approach. Still, we observe that CORES achieves comparable speed as SUGAR, and sometimes it is faster, e.g., with PTC or MUTAG. In terms of inference time, in Table 12, we can observe that even though CORES is still one order of magnitude slower than the *Full Models*, it is considerably faster than SUGAR.

Table 12: **Inference time comparison.** We show the average inference time in seconds along with the standard deviation of each model on each dataset. We use the GIN GNN architecture.

Dataset	Full Models		Sparse Models			
	Vanilla	DiffPool	SUGAR	GPool	CORES _N	CORES _E
BZR	0.0025 _{0.0001}	0.1447 _{0.0048}	-	0.0045 _{0.0003}	0.0540 _{0.0257}	0.0425 _{0.0011}
COX2	0.0026 _{0.0001}	0.1550 _{0.0093}	-	0.0062 _{0.0008}	0.1031 _{0.0349}	0.0526 _{0.0014}
DD	0.0028 _{0.0004}	-	-	0.0085 _{0.0006}	0.2262 _{0.0842}	0.1206 _{0.0016}
ENZYMES	0.0024 _{0.0000}	0.1992 _{0.0080}	0.1399 _{0.0094}	0.0063 _{0.0007}	0.0496 _{0.0014}	0.0625 _{0.0019}
MUTAG	0.0029 _{0.0001}	0.0596 _{0.0034}	0.0135 _{0.0036}	0.0065 _{0.0017}	0.0448 _{0.0056}	0.0415 _{0.0012}
NCI1	0.0022 _{0.0001}	1.3756 _{0.1246}	1.0187 _{0.1040}	0.0058 _{0.0004}	0.0530 _{0.0026}	0.1301 _{0.0602}
NCI109	0.0023 _{0.0001}	1.3685 _{0.0988}	0.9477 _{0.0132}	0.0055 _{0.0002}	0.0500 _{0.0006}	0.0563 _{0.0009}
PROTEINS	0.0025 _{0.0001}	0.3835 _{0.0619}	3.9375 _{0.0347}	0.0058 _{0.0007}	0.0437 _{0.0016}	0.0439 _{0.0008}
PTC	0.0028 _{0.0001}	0.1076 _{0.0050}	0.0398 _{0.0099}	0.0058 _{0.0005}	0.0395 _{0.0013}	0.0418 _{0.0005}